Biomaterials 247 (2020) 119975

Contents lists available at ScienceDirect

Biomaterials

journal homepage: www.elsevier.com/locate/biomaterials

The role of tumor-stroma interactions on desmoplasia and tumorigenicity within a microengineered 3D platform

Harpinder Saini[a], Kiarash Rahmani Eliato[b,c,d], Jaimeson Veldhuizen[a], Azadeh Zare[b,c,d], Mayar Allam[a], Casey Silva[a], Alex Kratz[a], Danh Truong[a], Ghassan Mouneimne[f], Joshua LaBaer[e], Robert Ros[b,c,d], Mehdi Nikkhah[a,e,*]

[a] School of Biological and Health Systems Engineering (SBHSE), Arizona State University, Tempe, AZ, 85287, USA
[b] Center for Biological Physics, Arizona State University, Tempe, AZ, 85287, USA
[c] Department of Physics, Arizona State University, Tempe, AZ, 85287, USA
[d] Center for Single Molecule Biophysics, Biodesign Institute, Arizona State University, Tempe, AZ, 85287, USA
[e] Virginia G. Piper Biodesign Center for Personalized Diagnostics, Biodesign Institute, Arizona, State University, Tempe, AZ, 85287, USA
[f] University of Arizona Cancer Center, Department of Cellular and Molecular Medicine, Tucson, AZ, 85724, USA

ARTICLE INFO

Keywords:
Tumor microenvironment
Tumor-stromal crosstalk
Desmoplasia
CAFs
Paracrine signaling
PDGF

ABSTRACT

The tumor microenvironment has been demonstrated to play a crucial role in modulating cancer progression. Amongst various cell types within the tumor microenvironment, cancer associated fibroblasts (CAFs) are in abundance, serving to modulate the biophysical properties of the stromal matrix, through excessive deposition of extracellular matrix (ECM) proteins that leads to enhanced tumor progression. There is still a critical need to develop a fundamental framework on the role of tumor-stromal cell interactions on desmoplasia and tumorigenicity. Herein, we developed a 3D microengineered organotypic tumor-stroma model incorporated with breast cancer cells surrounded by CAF-embedded collagen matrix. We further integrated our platform with atomic force microscopy (AFM) to study the dynamic changes in stromal stiffness during active tumor invasion.

Our findings primarily demonstrated enhanced tumor progression in the presence of CAFs. Furthermore, we highlighted the crucial role of crosstalk between tumor cells and CAFs on stromal desmoplasia, where we identified the role of tumor-secreted PDGF-AA/-BB on elevated matrix stiffness. Inhibition of the activity of PDGFRs in CAFs led to attenuation of stromal stiffness. Overall, our work presents a well-controlled tumor microenvironment model capable of dissecting specific biophysical and biochemical signaling cues which lead to stromal desmoplasia and tumor progression.

1. Introduction

Metastatic breast cancer is one of the leading causes of death amongst women across the United States [1]. It is now established that, besides tumor cells, the surrounding mammary tissue microenvironment plays a significant role in cancer progression from an early benign stage to invasive and metastatic phases [2]. The tumor-stroma is a complex milieu comprising of numerous cell types, with cancer associated fibroblasts (CAFs) in abundance [3]. Many studies have demonstrated that CAFs play a multifaceted role in tumor progression as they influence various hallmarks of cancer [3]. For instance, CAFs have been demonstrated to assist in epithelial to mesenchymal transition (EMT) of neoplastic cells by secretion of transforming growth factor β1 (TGF-β1) and interleukin 32 (IL-32) thereby enabling tumor invasion through the stroma [4,5]. CAFs also participate in immune regulation of the tumor microenvironment through secretion of tumor-promoting inflammatory cytokines including IL-6, IL-11, CXCL1 and CXCL2 [6]. Notably, CAFs are the key players, influencing the biophysical properties of the tumor microenvironment, through deposition of abundant extracellular matrix (ECM) fibers, including collagen as well as the cross-linking enzymes such as lysyl oxidase (LOX) which lead to elevated matrix stiffness and fiber reorganization [3], and in turn enhance tumor progression.

To date, *in vivo* models have been widely utilized to develop an in-depth understanding of the influence of CAFs on breast tumor growth and progression [7–9]. These studies have identified molecular mechanisms through which CAFs exhibit pro-tumorigenic activity; however, there are several limitations associated with *in vivo* models [10].

* Corresponding author. School of Biological and Health Systems Engineering (SBHSE), Arizona State University, Tempe, AZ, 85287, USA.
E-mail address: mnikkhah@asu.edu (M. Nikkhah).

https://doi.org/10.1016/j.biomaterials.2020.119975
Received 18 October 2019; Received in revised form 11 March 2020; Accepted 14 March 2020
Available online 21 March 2020
0142-9612/

In vivo models do not often enable measurements of the dynamic changes in biophysical properties of the activated stroma including ECM deposition and their resultant effects on the matrix stiffness. There have been only a few attempts using *in vivo* models to assess stiffness of cancerous tissues by utilizing biopsies and nanoindentation techniques [11,12]. Moreover, mechanistic dissection of the influence of specific classes of stromal cells on tumor progression and stromal desmoplasia cannot be achieved due to the presence of multiple confounding factors within the tumor microenvironment [10]. To that end, various three-dimensional (3D) *in vitro* tissue engineered and microfluidic models have been developed to study the influence of specific class of stromal cells, biochemical signaling factors or matrix properties on tumor progression, cancer cell invasion and drug resistance [13–22]. Microfluidic tumor models have demonstrated excellent capabilities in establishing causal relationships between the cancer cells and their surrounding stroma and the subsequent influence on tumor progression [10]. Alternatively, there have been a number of studies which have utilized tissue engineering approaches along with natural [23], synthetic [24] or composite hydrogels [25] to study tumor progression [26,27]. However, the focus for the majority of these studies has been centered on manipulating the biophysical properties of the tumor microenvironment and subsequently studying the influence of matrix properties on cancer cell behavior (i.e. invasion mode, drug resistance) [23,25,26]. Despite their significance, to our knowledge, none of the previous studies have quantitatively probed the *in situ* dynamic alterations in stromal ECM stiffness and remodeling to mechanistically assess desmoplasia, within the context of tumor-stroma crosstalk, during active tumor invasion.

In this study, we developed an open-top 3D tumor-stroma model with well-defined organotypic architecture incorporated with breast cancer cells surrounded by a CAF-embedded collagen hydrogel. We further integrated our microengineered tumor-stroma model with atomic force microscopy (AFM) to quantitatively assess the biophysical changes within the stromal matrix during tumor invasion, with high resolution and fidelity. To build our fundamental understanding on the role of tumor-stroma interactions on ECM remodeling, we assessed the changes in expression of profibrotic genes and cytokines by utilizing qRT-PCR and ELISA. Our results demonstrated that the presence of CAFs promoted invasion of tumor cells into the stroma, enhanced collagen fiber deposition and significantly elevated stromal matrix stiffness. Further studies indicated that the crosstalk between tumor cells and CAFs is necessary to induce significant changes in stromal matrix desmoplasia (i.e. stiffening and remodeling), as mono-culture of either cell type did not lead to biophysical alterations within the matrix. Our analysis notably highlighted the critical role of tumor secretome, specifically PDGF, on CAF-induced desmoplasia. Overall, this study has taken a step forward by building a microengineered model of tumor-stroma with well-defined organotypic architecture, coupled with AFM, to develop a fundamental framework on how cellular and molecular interactions of tumor-stroma (i.e. CAFs) govern tumor progression and desmoplasia.

2. Materials and Methods

Materials: Polydimethylsiloxane (PDMS, Sylgard 184 Silicon Elastomer Kit) was bought from Dow Corning to fabricate substrate holders and stamps (Fig. 1A). The PDMS holders were surface treated with 2-aminopropyl-trimethoxy-silane (APTMS, Catalog number 281788, Sigma) and glutaraldehyde (Catalog number 97064–908, VWR). Confocal dishes on the other hand were treated using Poly-D-Lysine (PDL, Catalog number P6407, Sigma) and glutaraldehyde. The PDMS stamps were rendered hydrogel repellant using 1% Pluronic-F 127 solution (Catalog number P2443, Sigma) in Deionized (DI) water. Rat tail collagen type 1 (Collagen-I) was purchased from Corning (Catalog number 354249) and Enzo Life Sciences (Catalog number 522–435) to fabricate the tumor-stroma model. The drug CP673451 (PDGFR inhibitor) was bought from Selleckchem (Catalogue number S1536) to inhibit the PDGF pathway within CAFs.

Cells: MDA-MB-231 cells (also referred to as MDA231 in Figures) transduced to stably express DsRed protein were obtained from Dr. Robert Ros's lab at Arizona State University. MCF7 cells transduced to stably express DsRed protein were a generous gift from Dr. Mouneimne' s lab at University of Arizona. For incorporation of breast fibroblasts in our study, we utilized the cell line HTB-125™, from ATCC, which was isolated from the region next to infiltrating ductal carcinoma and validated to exhibit fibroblast morphology as mentioned by the vendor. Based on our further analysis of this cell line, we confirmed positive expression for vimentin, with a subpopulation also expressing alpha smooth muscle actin (α-SMA), and minimal to no expression of pan cytokeratin, similar to that observed in cancer associated fibroblasts (CAFs) [3,28,29]. Thus, in our study we referred to this HTB-125™ cell line, with fibroblast morphology, as cancer associated fibroblasts (CAFs). These cells were obtained at passage 55 and were used between passage 56–60 for all our experiments. All the cells were maintained in DMEM 1X media supplemented with 10% (v/v) FBS, 1% (v/v) Pen/Strep and 1% (v/v) L-Glutamine. The cells were grown in T-75 flasks within an incubator maintained at 37 °C and 5% CO_2.

Antibodies/Growth Factors: Anti-pan-cytokeratin (1:100), anti-vimentin (1:100) and anti-α-smooth muscle actin (α-SMA, 1:100) antibodies were utilized. Phosphorylation of PDGFRs was visualized using pPDGFRα (Santa Cruz Sc-365464) and pPDGFRβ (AbCam ab5460) primary antibodies. To perform cell proliferation assay, Click-iT EdU Alexa Fluor 488 and Click-iT EdU Alexa Fluor 647 Imaging Kits (Thermo Fisher Scientific, Catalog number C10337, C10340) was used. To visualize cellular cytoskeleton, Alexa Fluor 488 phalloidin (Thermo Fisher Scientific) was used at 1:40 dilution. Goat secondary antibodies against mouse and rabbit primary antibodies were bought from Thermo Fisher Scientific and used at dilution range of 1:200–1:500.

2.1. PDMS surface treatment

The PDMS holders and stamps used to develop the micropatterned tumor-stroma model were designed using AutoCAD software. The dimensions of the holders were 8 × 8 mm such that they could fit within a single well of a 24-well plate. On the other hand, the PDMS stamps were incorporated with 300 μm microposts of 75 μm diameter with 250 μm center to center distance. Each stamp had an array of 15 × 15 microposts, in order to fabricate high density tumor entities within the model. PDMS holders and stamps were developed using soft lithography techniques, by casting off the silicon wafer, as explained previously [13]. For surface treatment of PDMS holders, they were cleaned using scotch tape and further treated with air-based plasma for the duration of 4 min and 30 s. The plasma treated holders were immersed into freshly prepared 2% (v/v) APTMS solution in 95% (v/v) ethanol and incubated at 60 °C for 1 h. Next, the APTMS solution was aspirated and the holders were immersed in 100% ethanol and ultrasonicated for 20 min at high frequency using water based ultrasonication. The ethanol solution was replaced with fresh 100% ethanol and washed 5 times consecutively with 10-min intervals on a plate shaker to remove residual APTMS. The treated holders were then incubated at 80 °C for 1 h. Next, the holders were incubated in 0.1% glutaraldehyde solution in DI water for 1 h. To remove excess glutaraldehyde, the treated holders were washed with DI water 5 times for 5-min intervals followed by overnight incubation at 80 °C. For stiffness measurement using AFM, we formed the tumor-stroma model on confocal dishes. The confocal dishes were treated with PDL at 1 mg/mL for 1 h followed by 1% glutaraldehyde treatment. The dishes were then incubated at 80 °C overnight. To make PDMS stamps protein resistant, they were immersed in 1% Pluronic F-127 solution in DI water overnight at 4 °C.

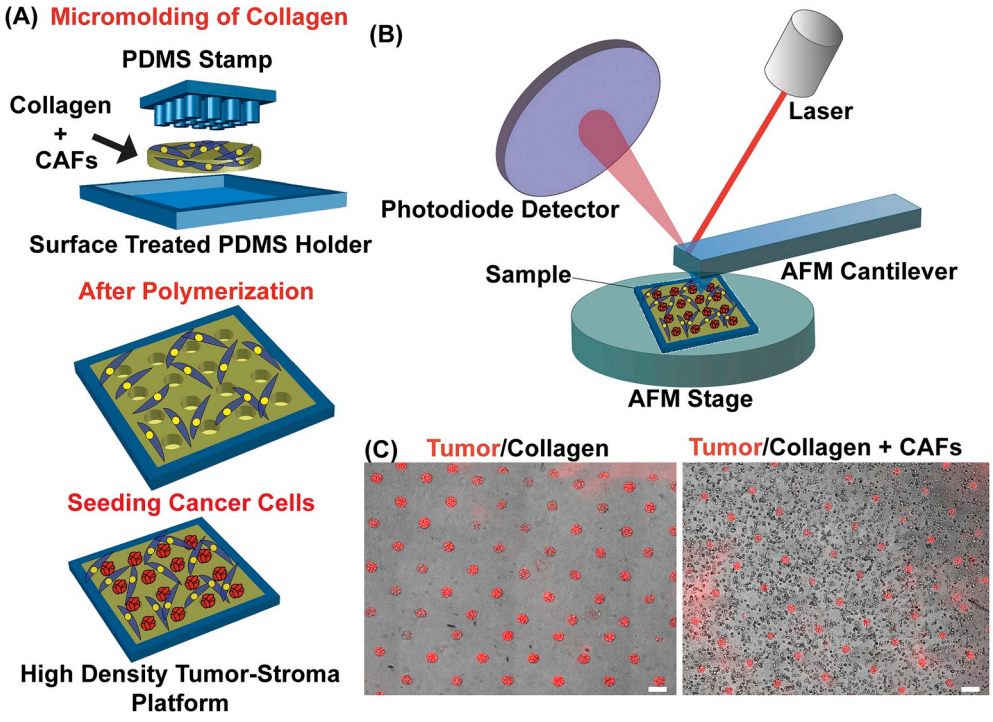

Fig. 1. Microengineering of 3D *in vitro* organotypic tumor-stroma model. (A) Schematic of microfabrication process of 3D tumor-stroma model with well-defined organotypic architecture. (B) Schematic of the integration of Atomic Force Microscopy (AFM) with the 3D tumor-stroma model. (C) Representative images showing successfully microfabricated 3D high density tumor-stroma model with mono-culture and co-culture groups. All scale bars represent 100 μm.

2.2. Fabrication of 3D tumor-stromal model

The micropatterned 3D tumor model, with well-defined architecture, was fabricated consistent with previous work reported by Nelson et al., with brief modifications [30]. Collagen-I was prepared at a final concentration of 4 mg/mL. For co-culture conditions, CAFs were mixed with collagen at a cell density of 2×10^6 cells/mL. PDMS stamps immersed in Pluronic solution were washed three times with DI water and the prepared collagen solution was added to each stamp and inverted on top of the PDMS holders. This assembly of inverted PDMS stamps coated with collagen solution on top of PDMS holders was then kept for polymerization for 30 min at 37 °C. Upon polymerization of the collagen, the stamps were lifted gently and the microwells were seeded with cancer cells at a density of 7×10^6 cells/mL for 3 min followed by washing with media as explained in previous protocols [30]. The cells were allowed to attach to collagen microwells by incubating the samples inside an incubator for 15 min before immersing in media within a 24-well plate similar to our previuos work [31].

2.3. Breast cancer invasion assay

In order to quantify breast cancer invasion, samples from all groups were imaged using Zeiss Observer Z1 inverted microscope, equipped with Apotome 2.0, on days 0, 2 and 4 of the culture. Using phase contrast and fluorescent microscopy, images were acquired of 2×2 tiles at 2 random locations of the sample. Next, the coordinates of the tumor cells were isolated within each image using ImageJ software (NIH), and a custom-written MATLAB code was utilized to perform Delaunay triangulation modelling similar to our previous reports [31]. The area of each triangle within each Delaunay plot as well as the standard deviation were calculated using MATLAB. Furthermore, we calculated average area of all triangles and quantified area disorder for each Delaunay plot using the following equation:

$$Area\ \ disorder = 1 - \left(1 + \left(\frac{standard\ \ deviation}{average\ \ area}\right)\right)^{-1}$$

Subsequently, the Migration Index was calculated, based on area disorder, through the following formula:

$$Migration\ \ Index = \frac{(Area\ \ disorder\ \ on\ \ Day\ \ 1 - Area\ \ Disorder\ \ on\ \ Day\ \ 3)}{Area\ \ disorder\ \ on\ \ Day\ \ 1}$$

MCF7 cluster areas were quantified using the ImageJ Analyze Particles plugin. The average cluster area for days 2 and 4 for all the samples in each condition were normalized with respect to day 0.

2.4. Cell proliferation assay

Cell proliferation was quantified using Click iT-Edu Imaging Kit. The assay was performed as per manufacturer's instruction. In order to quantify cancer cell proliferation, the $DsRed^+$ cells with EdU^+ nuclei were counted in ImageJ using the Cell Counter plugin. CAFs proliferation was quantified by counting the cells which were $DsRed^-$, with an EdU^+ nuclei. To calculate the percentage of proliferative cells, the EdU^+ cancer cells or CAF cells were divided by total number of cancer cells or CAFs, respectively.

2.5. Immunofluorescent staining

To perform immunofluorescent (IF) staining of our 3D samples, we first fixed them by using 300 μl of 4% (v/v) paraformaldehyde (PFA) for 30 min at room temperature. The fixed samples were then washed 2x with PBS-Glycine followed by1x wash with PBS. The samples were permeabilized in 300 μl of IF buffer containing 0.2% (v/v) Triton-X-100 + 0.1% (v/v) BSA +0.05% (v/v) Tween-20 + 7.7 mM NaN_3 in PBS for 30 min followed by 2x wash with PBS-Tween and 1x wash with PBS. The permeabilized samples were blocked using 300 μl of 10% (v/v) goat serum in IF buffer for 2 h followed by overnight incubation with 250 μl of primary antibodies at different dilutions. After removing primary antibodies, the samples were washed 3x times with PBS-Tween followed by 2x wash with PBS. The secondary antibodies were dissolved in 10% goat serum in IF buffer at appropriate dilutions and then added to the samples for 1 h followed by 3x wash with PBS-Tween and 2x wash with PBS for an interval of 10 min at a rocking station.

2.6. Atomic force microscopy (AFM)

An Asylum Research MFP-3D-BIO AFM was used to conduct the

force-indentation measurements to assess the dynamic changes of the stromal matrix stiffness during tumor progression. Team NanoTec LRCH-750 AFM probes with sphere-cone geometry were used. The spring constants (nominal k ~ 0.2 N m^{-1}) were determined using thermal energy dissipation method [32]. Samples were measured and imaged at 37 ˚C in 1X Hank's Balanced Salt Solution (HBSS) containing calcium and magnesium. The samples were also buffered with 25 mM HEPES to maintain their pH during the measurements. Quasi-static measurements with cantilever approach and retraction speed 2 μm s^{-1} were conducted to collect elastic modulus data. In a 90μm × 90 μm area in the middle of four micro-wells, a grid of 4 × 4 indentations were acquired by applying trigger force of 40–75 nN which resulted in 10–17 μm of indentation. The choice of trigger force was made to obtain desired indentation intervals. The first 10 μm of the force-indentation curves were fitted to a non-adhesive quasi-static contact model for a canonical indenter with a spherical tip that features continuous curvature at the transition point[65].

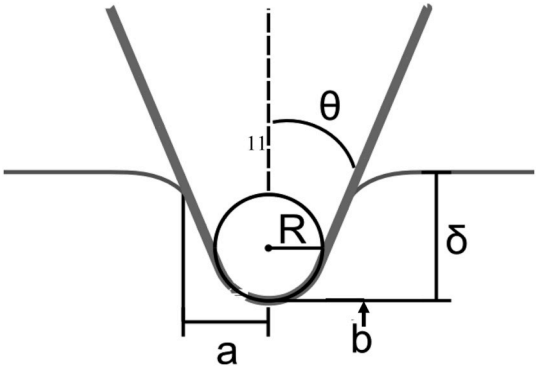

$$b = R\cos\theta \tag{1}$$

$$\delta(a \le b) = \frac{1}{2}a\ln\left(\frac{R+a}{R-a}\right) \tag{2}$$

$$F(a \le b) = \frac{E}{(1-\nu^2)}\left[\frac{1}{2}(a^2+R^2)\ln\left(\frac{R+a}{R-a}\right) - aR\right] \tag{3}$$

$$\delta(a > b) = a\ln\left(\frac{R+a}{\sqrt{R^2-b^2}+\sqrt{a^2-b^2}}\right) + a\cos^{-1}\left(\frac{b}{a}\right)\cot\theta \tag{4}$$

$$F(a > b) = \frac{E}{(1-\nu^2)}\left[a^2\cot(\theta)\cos^{-1}\left(\frac{b}{a}\right) + b\cot\theta\sqrt{a^2-b^2} - aR + \sqrt{(R^2-b^2)(a^2-b^2)} + a^2\ln\left(\frac{R+a}{\sqrt{R^2-b^2}+\sqrt{a^2-b^2}}\right) - \frac{R^2}{2}\ln\left(\frac{a^2R^2-(b^2-\sqrt{(R^2-b^2)(a^2-b^2)})^2}{b^2(R+a)^2}\right)\right] \tag{5}$$

Dynamic measurements, with the same probe approach and retraction speed, were conducted to collect viscoelastic data. In the same 90μm × 90 μm area of each quasi-static measurement a grid of 2 × 2 indentations were acquired by applying trigger force of 3–7 nN which resulted in 1.5–6 μm of quasi-static indentation. At the quasi-static indentations depth (δ_0) the oscillatory part of indentation ($\delta(\omega)$), with amplitude of 50 nm, at different angular frequency (ω) was applied by oscillating the z-piezo and measuring the oscillatory force respond of the sample. Later, amplitudes of force and indentation oscillation along with the phase lag between force-time and indentation-time curves were analyzed by the dynamic contact model derived from [Eq. (5)] to calculate the viscoelastic properties of sample (i.e. complex modulus) using the procedure described in [33].

$$G^*_{Spherecone}(\omega) = G'(\omega) + iG''(\omega) = \frac{1-\nu}{4a_{0,Spherecone}}\left(\frac{F(\omega)}{\delta(\omega)} - ib_{h=0}\omega\right) \tag{6}$$

where quasi-static contact radius $a_{0,Spherecone}$ is the solution of equation (6).

$$\delta_0 = a_0\ln\left(\frac{R+a_0}{\sqrt{R^2-b^2}+\sqrt{a_0^2-b^2}}\right) + a_0\cos^{-1}\left(\frac{b}{a_0}\right)\cot\theta \tag{7}$$

The dynamic experiment is carried out at frequencies of 1, 3.16, 10, 21.54, 31.62, 46.42, and 100 Hz.

2.7. Confocal reflectance microscopy

A Picoquant Microtime 200 confocal laser scanning microscope was used to obtain reflectance microscopy images. Each reflectance scan was 80 μm × 80 μm, 512 × 512 pixels (156nm/pixel) and took approximately 2.5 min. A 60 × , 1.1 NA, 1.5 mm W.D. water immerse objective was used (Olumpus LUMFL60×). Continuous blue diode laser (ex: 470 nm) was used to illuminate the sample and the reflected light was collected through a 30 nm pinhole and was detected by a single photon counting module (Picoquant PDM series). Intensity micrographs of the scans were constructed in the operating software (Picoquant SymphoTime). The amount of collagen fiber density was assessed by quantifying the mean pixel intensity of the confocal reflectance images using ImageJ software across various experimental groups throughout the culture period.

2.8. Real time cell tracking

To quantify tumor cell migration pattern and parameters, we performed 12 h of live cell tracking at the time period of 72 h of the culture. The movies were acquired using Zeiss Observer Z1 inverted microscope equipped with Apotome 2.0. The microscope stage was surrounded by an in-house built incubator integrated temperature control unit and CO_2 supply to maintain optimum culture conditions (33–34˚C and 5% CO_2). The z-stack images were acquired every 45 min using 10X objective across a depth of 50–60 μm. The images were then analyzed using a cell tracking script within MATLAB (Cell Tracker, Budapest, Hungry). Each cell was manually tracked frame-by-frame to record the cell coordinates. Using the software, cell velocity and persistence were calculated for each cell across all the samples. We analyzed 15 cells per movie with duplicate replicates in each experimental condition. Each experiment was repeated three times such that 90 cells were tracked for each condition. The cell tracks were obtained using ibidi Chemotaxis and Migration Tool with an ImageJ plugin.

2.9. Conditioned media experiments

To perform conditioned media (CM) experiments, MDA-MB-231 and MCF7 cells were cultured within the microengineered model in both mono-culture and co-culture conditions for 4 days and media was collected on day 2 and 4 of the culture. The CM was then centrifuged at 4000 RPM for 10 min at 4 ˚C to remove any cell debris and further stored in −80 ˚C. Next, CAFs were cultured in mono-culture condition within the microengineered model for 4 days. Right after initial AFM measurement of the CAF-only samples on day 0, day 2 CM collected from tumor mono-culture and co-culture samples was added. The measurements were repeated on day 2 for the same samples followed by incubation in day 4 CM and a final measurement on day 4.

2.10. Western blot

Western blot was performed according to a protocol provided by Bio-Rad. Briefly, cells were lysed with a solution containing protease inhibitors. These samples were then denatured in loading buffer.

Proteins were separated with Gel Electrophoresis using a 10% polyacrylamide gel. The proteins were transferred to a PVDF membrane using Bio-rad Trans Blot Turbo blotting system. Membranes were blocked in 5% BSA and stained using mouse primary antibody and 800 nm tagged goat anti-mouse secondary antibody. These membranes were then imaged using the licor Odyssey imager. For all the blots, vinculin was used as loading control.

2.11. qRT-PCR

Cells were isolated from the 3D microengineered tumor model by incubating the samples in 2 mg/mL collagenase I dissolved in 1X PBS for 30 min inside a 37 °C incubator. The samples were then mechanically digested by pipetting. The collagenase I solution was then collected and centrifuged to form a cell pellet. The cells were then mixed with 300 μl RNA lysis buffer (Zymo) to lyse the cells and collect total RNA. The RNA was purified using Zymo's Micro RNA Prep Kit. Specifically, to digest genomic DNA, isolated RNA was subjected to DNAse I treatment. The quality and quantity of RNA was confirmed using NanoDrop . Using 1 μg as the starting RNA template, cDNA was prepared using Quantabio cDNA Supermix. The qRT-PCR was performed by using Luminaris Color HiGreen qPCR Master Mix (Thermo Scientific) with appropriate controls as per manufacturer's Instructions. The qPCR plates were analyzed using qTower 2.0 (Analytik Jena US). The primer sequences for various genes have been detailed in the supplementary documents.

2.12. Quantification of cytokines within our 3D tumor model

The relative expression of cytokines was measured within the 3D microengineered samples by utilizing a custom-made Quantibody array from Raybiotech. The custom-built array was used to specifically study the expression levels of IL-4, IL-13, PDGF-AA, PDGF-BB, PDGF-AB, PDGF-CC and TGF-β. To perform the assay, FBS-containing CM was collected on day 4 from our samples and centrifuged at 4000 RPM for 10 min at 4 °C. The supernatant was collected and stored at −80 °C until further use. Due to the presence of serum in CM, the media was diluted 5-fold using sample diluent. A media blank was also added to samples to normalize the concentration of various cytokine. The assay was performed as per the manufacturer's instruction and then shipped to Raybiotech for fluorescent value measurement and extraction.

2.13. Statistical analysis

All of the experiments were repeated three times with triplicate samples per condition. The invasion and elastic modulus data were analyzed using two-way ANOVA followed by appropriate post hoc test. The standards for cytokine expression data were plotted by using Sigmoidal 4PL curve in Graph Pad Prism and unknown concentrations of the samples were interpolated from these curves. The relative expression was compared across samples by using one-way ANOVA followed by Dunnet multiple comparison test. All other data were analyzed using paired *t*-test. P-value less than 0.05 was considered significant for all the results. The statistical analyses and data representation were performed using GraphPad Prism v 7.0. All the data were presented as Mean ± Standard Deviation.

3. Results

3.1. Fabrication of the high-density 3D breast tumor-stroma model

In order to spatially organize cancer cells surrounded by CAF-embedded stroma within the 3D microengineered tumor-stroma model, we utilized a micropatterning technique. Specifically, the open-top model was fabricated by using PDMS stamps and micro-molding technique to construct a high-density array of microwells within collagen hydrogel (Fig. 1A) similar to our previous report [31]. The stromal region of the model comprised a CAF-embedded collagen matrix while the tumor regions were seeded by breast cancer cells (MDA-MB-231, MCF7) within the microwells (Fig. 1A). The model was further integrated with AFM to assess the *in situ* biophysical properties of the stroma, specifically matrix stiffness, during active invasion (Fig. 1B). We were able to successfully fabricate the proposed model with mono-culture and co-culture conditions, confirmed by spatial localization of cancer cells within the microwells ($DsRed^+$) surrounded by collagen matrix in either the absence or presence of CAFs (Fig. 1C).

All three cancer cell types (MCF7, MDA-MB-231 and CAFs) used in this study were immortalized cell lines. CAFs (HTB-125™ line from ATCC) were isolated from the breast tissue peripheral to the infiltrating ductal carcinoma, a region around the tumor core, utilized by various other studies to isolate CAFs due to their dynamic interaction with the tumor cells [9,29]. Prior to their incorporation within the model, we primarily characterized the phenotype of CAFs and other cell lines. We studied the expression of specific proteins including α-smooth muscle actin (α-SMA, myofibroblast phenotype marker), vimentin (mesenchymal marker) and pan-cytokeratin (epithelial marker) using IF and Western blot techniques. Our results confirmed that while vimentin was expressed by MDA-MB-231 and CAFs, pan-cytokeratin was expressed by MDA-MB-231 and MCF7 cells (Supplementary Fig. 1). On the other hand, α-SMA was only expressed by CAFs and was absent in MDA-MB-231 and MCF7 cells (Supplementary Figs. 1A and B). Upon performing densitometry analysis, we found that the adjusted density values for two biological replicates of CAFs shown in Supplementary Fig. 1B was ~0.97 ± 0.04. As shown by IF, not all of the CAFs had positive α-SMA expression (Supplementary Fig. 1A). Such heterogeneity in α-SMA expression across the CAFs population has also been previously reported for CAFs isolated from different patient samples [3,29]. Multiple studies have also highlighted that such a discrepancy in marker expression is due to the presence of highly heterogenous population of CAFs as they arise from different sources including transformation of normal fibroblasts, differentiation from epithelial cells, smooth muscle cells and adipocytes [34,35]. Additionally, no marker has been identified which is unique to the CAFs population as most of the CAF-related markers are shared with other cell types including normal fibroblasts, tumor cells and immune cells [34]. Currently, CAFs are distinguished from normal fibroblasts based on expression of a myofibroblast phenotype, upregulated ECM production and their tumor promoting capabilities; characteristics displayed by the fibroblasts used in our study as well [3,28,29,36,37]. Therefore, our data along with previous reports suggest that the immortalized cell line isolated from infiltrating ductal carcinoma (HTB-125™) used for this study exhibited CAF-like phenotype.

3.2. Tumor invasion and progression

To visualize the effect of CAFs on breast tumor cell invasive capabilities, we initially performed phase contrast microscopy and fluorescent imaging across the culture period of 4 days. Our results demonstrated single cell invasion of MDA-MB-231 cells into the stroma across all experimental conditions (Fig. 2A). While in mono-culture condition, these highly invasive cancer cells aggregated near the microwells, they demonstrated cellular scattering within the stroma when cultured with CAFs ($DsRed^+$, Fig. 2A, Supplementary Fig. 2A). To further quantify cell scattering, we utilized a mathematical model known as Delaunay Triangulation [38]. As shown in the Delaunay plots in Fig. 2B, MDA-MB-231 cells initially localized close to each other within microwells, as can be observed from many small area triangles located close to the microwells in both mono-culture and co-culture conditions on day 0. Large area triangles connected nodes between cells from different microwells. However, by day 4 of the culture period, tumor cells scattered within the stroma, away from the microwells in co-culture condition leading to a homogenous triangle area distribution

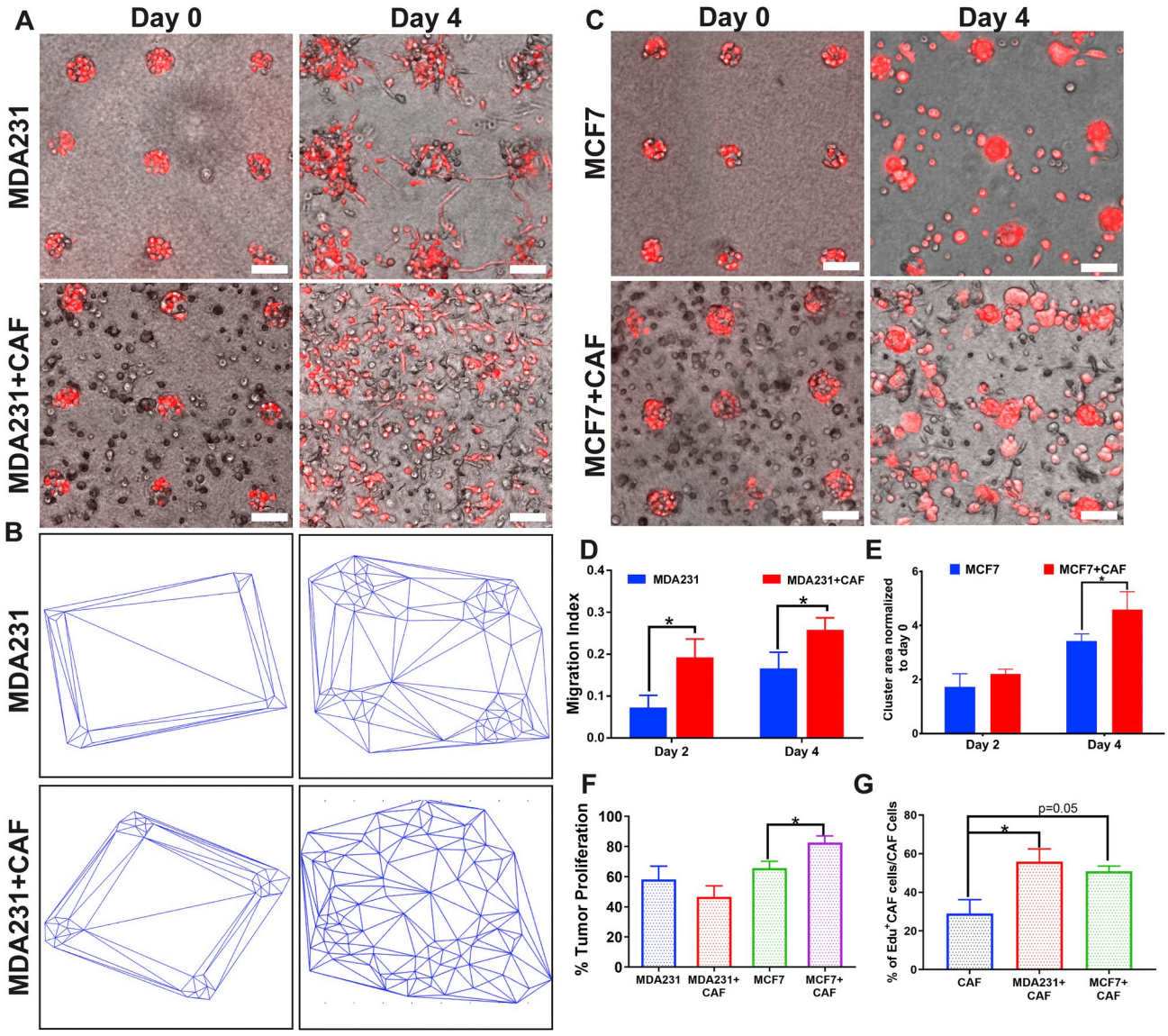

Fig. 2. Tumor cell invasion and proliferation analyses in mono-culture and co-culture conditions. (A) Representative phase contrast and fluorescent images across mono-culture and co-culture group of MDA-MB-231 cells with CAFs over culture period of 4 days. (B) Representative color-coded Delaunay triangulation graphs across experimental groups demonstrating MDA-MB-231 cell scattering in presence of CAFs. (C) Representative phase contrast and fluorescent images across mono-culture and co-culture group of MCF7 cells with CAFs. (D) Migration Index of MDA-MB-231 cells in mono-culture and co-culture conditions. (E) Quantified cluster area of tumor cells across experimental groups for day 2 and day 4 normalized to day 0. (F) Quantification of percentage of EdU^+ cancer cells between mono-culture and co-culture groups for MDA-MB-231 and MCF7 cells with CAFs. (G) Quantification of percentage of EdU^+ CAFs in mono-culture and co-culture groups. All scale bars represent 100 μm * represents p value $<$ 0.05. (For interpretation of the references to color in this figure legend, the reader is referred to the Web version of this article.)

(Fig. 2B). In contrast, in mono-culture group, these cells aggregated near the microwells through the duration of culture period of 4 days, as observed by presence of small size triangles between cells around the same microwell and the persistence of large area triangles between cells from different microwells (Fig. 2B). To quantify cell dispersion across mono-culture and co-culture groups, a custom metric migration index was calculated (see Materials and Methods) using triangulation graphs. As shown in Fig. 2D, the migration index of MDA-MB-231 cells upon co-culture with CAFs was significantly higher than the mono-culture condition on days 2 and 4. These quantifications further confirmed our imaging observations, demonstrating enhanced invasion abilities of MDA-MB-231 cells in presence of CAFs.

In contrast to single cell migratory behavior of MDA-MB-231 cells, less invasive MCF7 cells depicted colony forming tendencies within the 3D model, leading to cell aggregation thereby limiting triangulation analysis (Fig. 2C, Supplementary Fig. 2B). During the culture period of 4 days, MCF7 cells clustered and filled up the microwells, where they were initially seeded, across all experimental groups (Fig. 2C). While in mono-culture, these less invasive cells invaded the stroma in the form of single cells or small clusters, they formed large clusters within the co-culture group throughout the stroma (Fig. 2C, Supplementary Fig. 2B). Quantification of normalized cluster area on day 2 and 4 suggested that the clustering abilities of MCF7 cells significantly enhanced in the presence of CAFs (Fig. 2E). 3D F-actin stained images (Supplementary Fig. 2) further confirmed that while MDA-MB-231 cells invaded across different planes of the 3D hydrogel matrix, MCF7 cells invaded as a single sheet layer on top of the collagen hydrogel across all the conditions. Such a difference in invasion abilities between these two types of tumor cells can be attributed to their genomic make up, which is maintained within 3D culture, as suggested by previous reports [39].

Overall, our results demonstrated that while MDA-MB-231 cells enhanced their single cell invasion abilities, MCF7 cells depicted a higher tendency towards cluster formation and expansion within the stroma in the presence of CAFs.

3.3. Tumor and stromal cell proliferation

Many tumor cells depict the invasion-proliferation dichotomy phenomenon such that highly migratory cells lose their proliferative phenotype during invasion [40]. In this context, we utilized EdU assay to isolate the influence of CAFs on cancer cell migration from proliferation and to identify dividing tumor cells. As shown in Supplementary Fig. 3, dividing cancer cells were marked for newly synthesized DNA (co-expressing DsRed and GFP), demonstrating proliferation across all experimental groups. Quantification for EdU^+ tumor cells suggested an enhanced proliferative behavior of MCF7 cells upon co-culture with CAFs as compared to their mono-culture (Fig. 2F). On the other hand, MDA-MB-231 cells did not demonstrate any significant change in their proliferation rate when cultured with CAFs (Fig. 2F). Such a stark difference in proliferative behavior of different breast tumor cells, combined with previous invasion observations (Fig. 2A–E), potentially suggests that while CAFs enhanced MDA-MB-231 cells invasion, they primarily influenced the proliferation capacity of MCF7 cells in our platform.

In addition to tumor cell proliferation, we also investigated CAFs proliferation across different co-culture groups within the micro-engineered 3D tumor-stroma model. CAFs ($DsRed^-$) depicted an enhanced proliferation in the presence of both MDA-MB-231 and MCF7 cells (Fig. 2G, Supplementary Fig. 4). These results are consistent with previous clinical studies where metastatic cancerous tissues were observed to have a high quantity of α-SMA-expressing CAFs as compared to non-metastatic tissue [41][66], suggesting that the crosstalk between tumor and stromal cells can profoundly influence their proliferative behavior.

3.4. Real time tracking of tumor cells

While we demonstrated that the presence of CAFs influenced the proliferation and invasion capacities of tumor cells, we further studied the migration patterns through real-time cellular tracking (Fig. 3). As shown in Supplementary Movies 1 and 2, MDA-MB-231 cells migrated as single cells across mono-culture and co-culture conditions. The representative cell tracks further demonstrated enhanced dissemination of MDA-MB-231 tumor cells in the presence of CAFs as compared to their mono-culture (Fig. 3A). Using a live cell tracking script, we quantified MDA-MB-231 cell speed and persistence in all the experimental groups (Fig. 3B). Our analysis for the bulk population of MDA-MB-231 cells demonstrated no significant difference in cell migration speed between the mono-culture and co-culture conditions (Fig. 3C). However, when the speed of individual tumor cells was considered, we observed that about 80% of tumor cells migrated at a baseline cell speed (≤ 0.16 μm/min) in mono-culture as opposed to 58% in the co-culture condition (Fig. 3B). Upon co-culture with CAFs, a significant number of tumor cells enhanced their migratory characteristics and invaded the stroma at an increased cell motility speed of ≥ 0.2 μm/min (38% in co-culture condition vs 20% in mono-culture condition, Fig. 3B, D). We also studied MDA-MB-231 cell persistence, indicative of directionality of cell motion, and observed no significant difference for the bulk population of tumor cells between mono-culture and co-culture conditions (Fig. 3E). Upon analysis of distribution of cell persistence between the mono- and co-culture groups, we observed an increased number of MDA-MB-231 cells exhibiting high persistence (≥ 0.3) in co-culture condition (Fig. 3F). Overall, our results demonstrated that when MDA-MB-231 cells are co-cultured with CAFs, a significant population of tumor cells acquire enhanced invasion characteristics, upregulating their cell speed and persistence.

Supplementary video related to this article can be found at https://doi.org/10.1016/j.biomaterials.2020.119975

Similar real-time analysis was also performed on MCF7 cells (Fig. 3 and Supplementary Movies 3, 4). While MDA-MB-231 cells migrated as single cells, interestingly, we observed that MCF7 cells on the other hand demonstrated a high tendency in forming clusters across all experimental groups consistent to our previous observations (Fig. 2C, Supplementary Fig. 2). As can be observed in Supplementary Movies 3 and 4, many cells clustered with other cells during the 12-h tracking period, thereby increasing the overall cluster size. Similarly, many cells during this period demonstrated a tendency to proliferate and thus upon division followed their individual paths, rendering it difficult to quantify individual cells' migratory characteristics. Therefore, we limited our analysis to the single cells that neither proliferated nor clumped during the 12-h migration period (see Methods). Representative cell tracks for each condition suggested no noteworthy changes in MCF7 tumor cells dissemination pattern, (Fig. 3A). Further analysis demonstrated no significant differences in cell speed and persistence between mono-culture and co-culture groups (Fig. 3G, I). Similar to MDA-MB-231 cells, the histogram of cell speed distribution for MCF7 cells also exhibited no significant differences between mono-culture and co-culture groups in terms of cell speed (Fig. 3B, H). However, our analysis showed a slight decrease in number of cells with high persistence in the co-culture condition as compared to mono-culture condition (Fig. 3J, p-value = 0.042). Thus, our findings overall indicate that while CAFs influenced the migration of MDA-MB-231 cells by increasing the cell speed and persistence of a select population of tumor cells, MCF7 cells on an average exhibited more cluster tendency formation and proliferation in the presence of CAFs.

Supplementary video related to this article can be found at https://doi.org/10.1016/j.biomaterials.2020.119975

3.5. Characterization of stromal ECM remodeling

A major step forward in our 3D microengineered tumor model lies within its ability to assess *in situ* biophysical properties of the stromal ECM, including collagen deposition and matrix stiffness due to stromal-tumor crosstalk. To assess stromal desmoplasia, particularly collagen matrix deposition and stiffness, within our platform, we utilized AFM along with 3D confocal reflectance microscopy. As shown in Fig. 4A and B, collagen fiber density did not change significantly throughout the culture period of 4 days in the mono-cultures of both MDA-MB-231 and MCF7 cells as well as in the mono-culture of CAFs (Supplementary Fig. 5A). However, upon co-culture with CAFs, collagen expression gradually increased on days 2 and 4 of culture (Fig. 4A and B). A similar observation was made from the quantification of collagen fiber density as shown in Supplementary Table 1. Our assessment demonstrated that the mean pixel intensity of the collagen fibers was similar across all the experimental groups on day 0 (Supplementary Table 1). While in the mono-cultures of either tumor cells or CAFs, the pixel intensity of collagen fiber density across the culture period remained unchanged, the intensity of collagen fiber density increased by 1.29 and 1.31 times in co-culture conditions of MDA-MB-231 and MCF7 cells with CAFs respectively. Such an increase in collagen deposition further influenced stiffness of the stroma, which was quantified by measurement of the elastic modulus of the matrix using AFM. As shown in Fig. 4C, neither the mono-culture of tumor cells (MDA-MB-231, MCF7) nor CAFs induced any change in the matrix stiffness across the culture period. Interestingly, only during the co-culture of tumor and stromal cells, a significant increase in elastic modulus was observed (Fig. 4C). Specifically, when MDA-MB-231 cells were co-cultured with CAFs, the matrix stiffness increased from 0.89 ± 0.4 KPa on day 0 to 2.85 ± 1.15 KPa on day 4. Similarly, upon co-culture of MCF7 cells with CAFs, elastic modulus of the matrix increased from 1.474 ± 0.515 KPa to 3.543 ± 0.41 KPa across the culture period of 4 days. Our results also showed that while the increase in the elastic modulus of ECM in co-

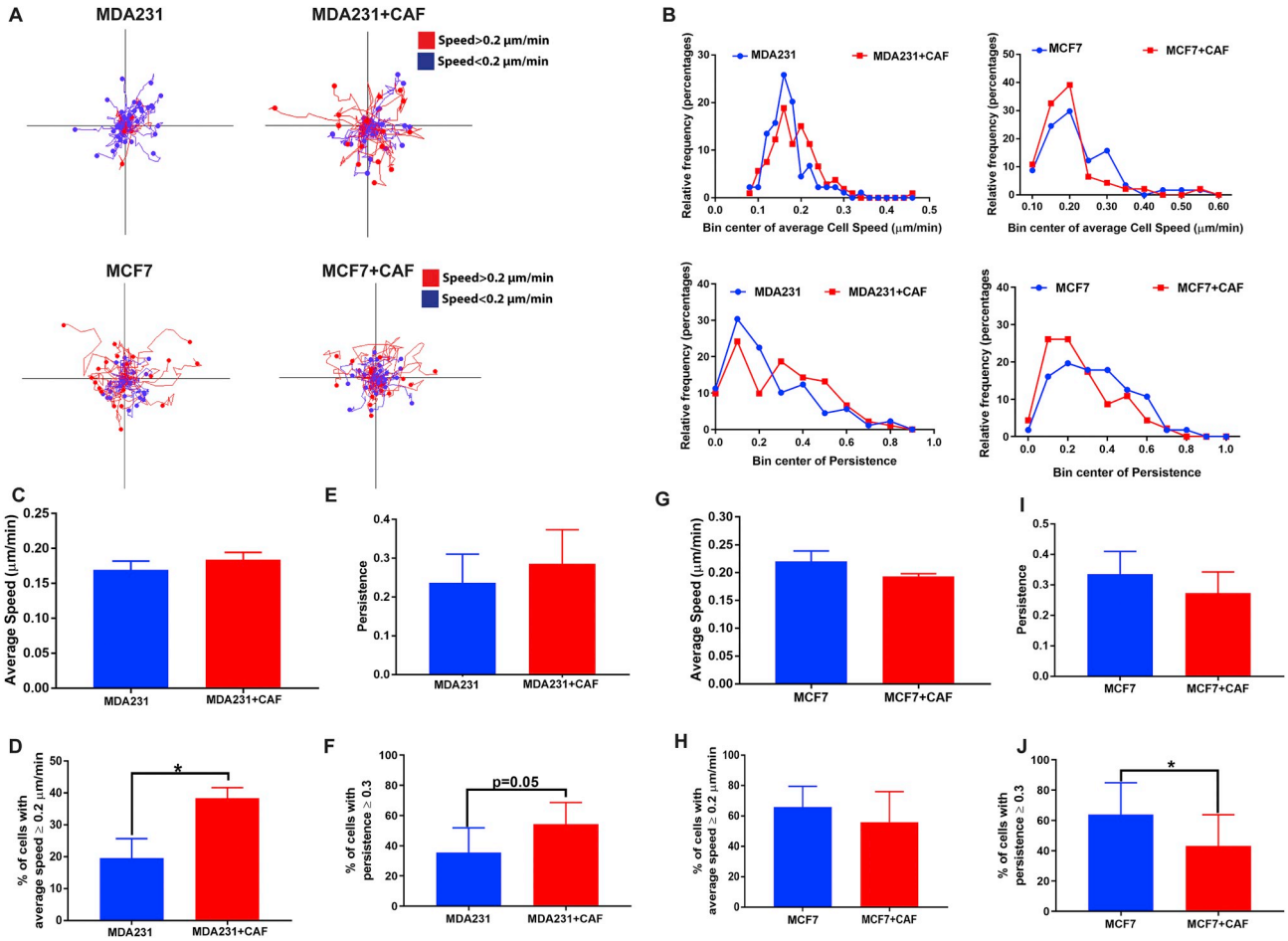

Fig. 3. Real time tumor cell tracking analyses. (A) Representative cell tracks across mono-culture and co-culture group for MDA-MB-231 and MCF7 cells. (B) Histogram of cell speed and persistence for MDA-MB-231 and MCF7 cells within each condition. (C) Average speed of MDA-MB-231 cells across all culture conditions. (D) Quantification of percentage of MDA-MB-231 cells with average speed greater than or equal to 0.2 μm/min across all groups. (E) Average persistence of MDA-MB-231 cells. (F) Quantification of percentage of cells with average persistence greater than 0.3 across all groups. (G) Average of MCF7 single cells speed across all culture conditions. (H) Quantification of percentage of MCF7 cells with average speed greater than or equal to 0.2 μm/min across all groups. (I) Average persistence of MCF7 cells. (J) Quantification of percentage of MCF7 cells with average persistence greater than 0.3 across all groups. * represents p value $<$ 0.05.

culture condition of MDA-MB-231 cells was progressive across culture period, it was delayed for MCF7 cells until day 4 (Fig. 4C). Consistent with these findings, the matrix stiffness was observed to be significantly higher in different co-culture groups (MDA-MB-231 + CAF, MCF7 + CAF) as compared to the respective mono-culture of tumor cells or CAFs on day 4 (Supplementary Figs. 6A and B). Despite the difference in invasive capabilities of the tumor cells used in the study (highly invasive MDA-MB-231 cells and less invasive MCF7 cells), no significant differences were observed in the elastic moduli of the ECM between the two co-culture groups across the culture period. Thus, our results overall demonstrate that the crosstalk between tumor cells and CAFs is necessary to induce stromal desmoplasia. Specifically, the tumor cells of varied tumorigenicity used in this study are able to interact with CAFs equivalently to induce matrix deposition and enhance stromal desmoplasia.

To further our understanding of the biophysical changes caused by tumor-stromal crosstalk, we further analyzed the viscoelastic properties of the stromal matrix. In dynamic indentation experiments, we quantified the storage (G′) and loss moduli (G″), as well as the loss tangents (G″/G′) of stromal matrix for different experimental groups (Supplementary Figs. 5B, C, 7). Our analysis demonstrated lower values of loss moduli G″ as compared to storage moduli G′ throughout all the groups across the entire probed frequency range, indicating a more solid-like behavior of the matrix (Supplementary Figs. 5B, 7A, C). The model, as determined by the loss tangent (G″/G′) (Supplementary Figs. 5C, 7B, D), exhibited values in the range of 0.1–0.3, clearly indicating domination of the elastic properties. As expected from the quasistatic experiments described above (for isotropic materials with a Poisson ration of 0.5), the elastic modulus E is three times the shear storage modulus G′. Our results thus demonstrated a significant increase in the storage modulus (G′) when MDA-MB-231 cells or MCF7 cells were co-cultured with CAFs as compared to their respective tumor mono-cultures on day 4, suggesting an increase in the elastic properties over viscous properties of the stromal matrix (Supplementary Figs. 7A and C).

3.6. Assessment of expression of matrix-related genes

To further probe the mechanism of ECM remodeling at the molecular level, we performed qRT-PCR on matrix-related genes including alpha I type I collagen (COL1A1), alpha I type III collagen (COL3A1), fibronectin (FN), lysyl oxidase (LOX) and transforming growth factor beta 1 (TGF-β1) across different experimental groups (Fig. 4D and E). To better understand gene expression in the co-culture samples as a whole similar to the *in vivo* condition, we did not sort or separate the tumor cells or CAFs in co-culture groups but rather compared the expression of the mixed population of the cells with the mono-culture samples of respective tumor cells and CAFs as controls (Fig. 4D and E). Similar to imaging of collagen fibers, gene expression analyses demonstrated significantly higher expression of matrix genes including

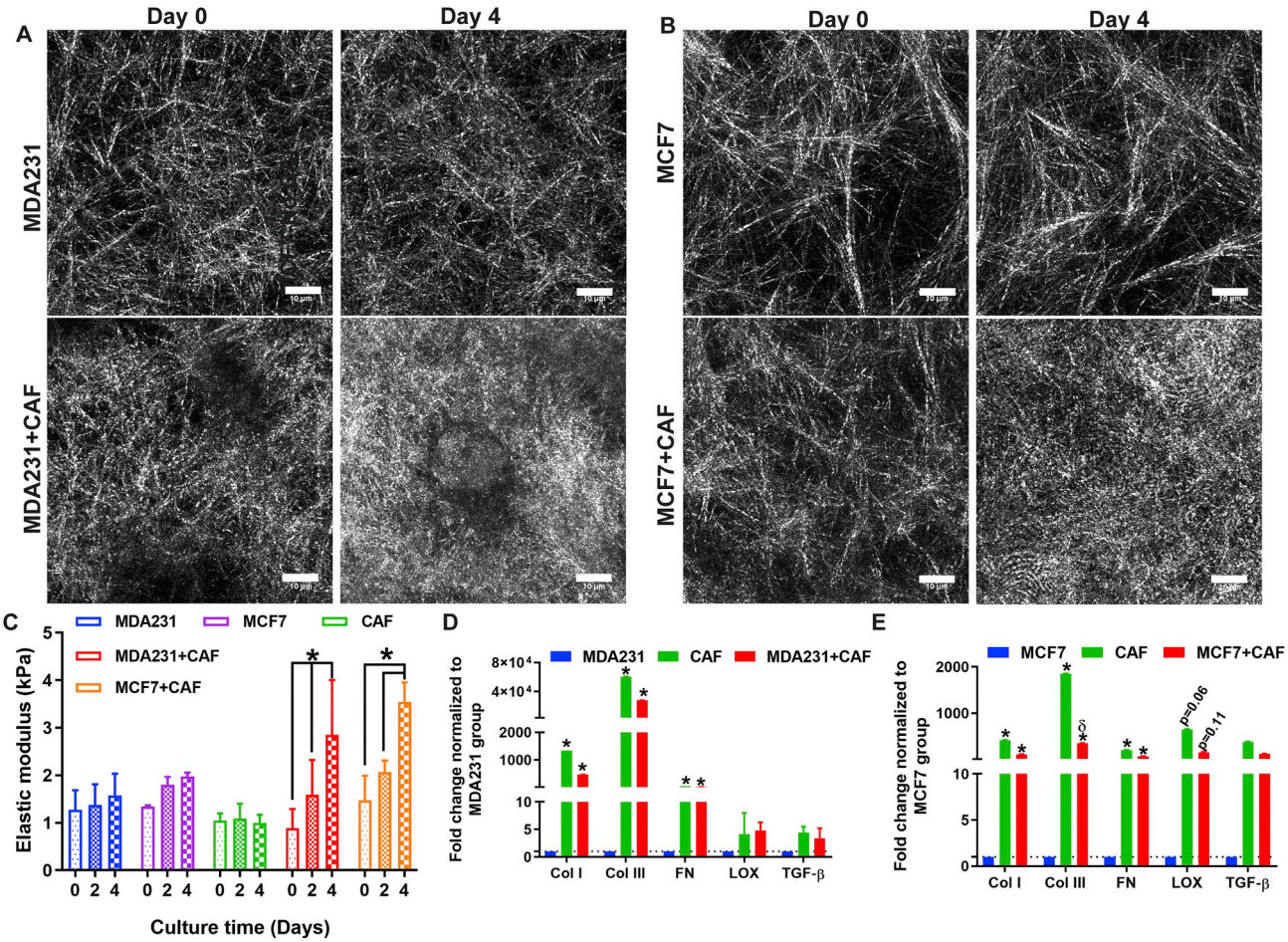

Fig. 4. Assessment of stromal ECM stiffness, remodeling and upregulation of matrix-related genes. (A),(B) Representative back reflection confocal images showing collagen deposition across experimental group of MDA-MB-231 and MCF7 cells over the culture period of 4 days. (C) Quantified elastic modulus of stromal ECM across different culture conditions through 4 days of culture. All scale bars represent 10 μm. (D),(E) Quantification of RNA expression for various matrix-related genes in co-culture groups of MDA-MB-231 or MCF7 cells with CAFs compared to the respective mono-culture of tumor cells as well as mono-culture of CAFs. * represents p value < 0.05.

COL1A1, COL3A1 and FN in co-culture samples of tumor cells with CAFs as compared to mono-culture of respective tumor cells (Fig. 4D and E). We further observed significantly higher expression of COL1A1, COL3A1 and FN in mono-culture of CAFs as compared to mono-culture of either tumor cell line. Upon additional analysis, we found no significant differences among expression levels of the matrix genes between mono-culture of CAFs and co-culture groups thereby suggesting that CAFs, not tumor cells, are the primary source of upregulation of these matrix-related genes within the co-culture condition, underlining the CAF-specific role in ECM remodeling.

3.7. The influence of tumor secretome on ECM remodeling and CAFs phenotype

Since ECM stiffness analyses demonstrated the necessity of tumor cells and CAFs interaction to induce stromal remodeling, we next aimed to dissect the possible mode of this interaction between these two cell types. Specifically, we studied whether soluble factors signaling between tumor cells and CAFs are responsible for stromal desmoplasia over the culture period. To perform these studies, we collected conditioned media (CM) from different experimental groups of MDA-MB-231 and MCF7 cells and subsequently added the respective tumor cell CM to the mono-culture of CAFs embedded in collagen matrix followed by assessment of elastic modulus of the matrix. As shown in Fig. 5A, C, collagen fiber density and matrix stiffness of the CAF-only group was significantly enhanced when CM from mono-culture of MDA-MB-231 cells was added to the samples (0.82 ± 0.24 KPa on day 0 to3.45 ± 0.64 KPa on day 4). Similarly, when CAFs were incubated with CM obtained from mono-culture of MCF7 cells, the matrix stiffness significantly enhanced from 0.62 ± 0.3 KPa on day 0 to 2.2 ± 0.2 KPa on day 4 (Fig. 5B, D). These results are therefore indicative of the crucial role of paracrine signaling between tumor cells and CAFs to induce stromal desmoplasia. Surprisingly, our results demonstrated no significant change in matrix stiffness in CAF mono-culture when incubated with CM obtained from the co-culture groups of either MDA-MB-231 or MCF7 cells (Fig. 5). We speculate that CAFs present in the co-culture groups consume the tumor-secreted pro-fibrotic factors by ligand-receptor internalization thereby limiting their availability within the collected CM [42,43]. Such an unavailability of potential pro-fibrotic factors in co-culture CM possibly explains the insignificant change in matrix stiffness when incubated on CAF mono-culture samples across the culture period. Overall, we speculate that the tumor cells secrete soluble factors that are sensed by CAFs to induce stromal desmoplasia, and which upon binding with receptors on CAFs get internalized by the process of ligand-receptor complex internalization [43].

After establishing a significant role of soluble factor signaling in modulation of the biophysical properties of the stromal matrix by CAFs, we also analyzed CAF proliferation upon incubation with CM obtained from the different experimental groups of MDA-MB-231 and MCF7

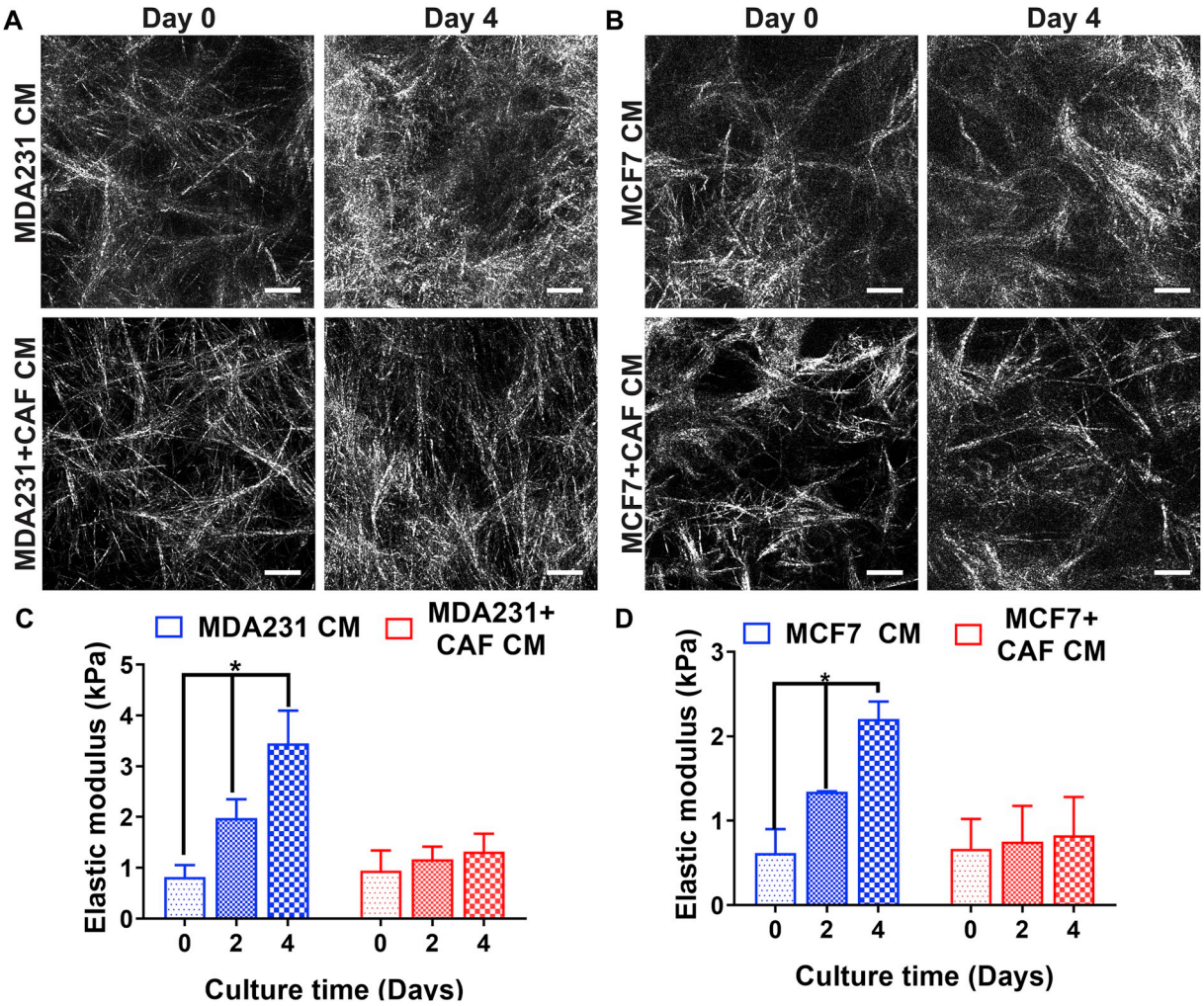

Fig. 5. Conditioned media (CM) assay and assessment of stromal ECM remodeling and stiffness. (A), (B) Representative confocal reflectance images showing deposition of collagen fibers when CAF-embedded hydrogel are incubated with CM obtained from various mono-culture and co-culture groups. (C) Quantified elastic modulus of ECM for the CAF-embedded matrix upon incubation with CM from mono-culture and co-culture groups of MDA-MB-231 cells. (D) Elastic modulus of the CAF-embedded matrix when incubated with CM from various groups of MCF7 cells. All scale bars represent 20 μm * represents p value $<$ 0.05.

cells. As shown in Supplementary Fig. 8A, although CAFs demonstrated proliferation under all the conditions, there were no significant differences in proliferative behavior of CAFs when incubated with CM obtained either from mono-culture or co-culture group of both MDA-MB-231 and MCF7 cells as well as those cultured in regular DMEM-based media (Supplementary Fig. 8B). Similar reassessment was also performed for expression of matrix genes in CAFs incubated with CM obtained from various experimental groups. Our results demonstrated that CAFs did not exhibit significant changes in expression of any of the assayed matrix genes when incubated with CM of mono-culture and co-culture groups (Supplementary Figs. 8C and D). Therefore, our results demonstrated that the tumor secretome did not change either the level of matrix-related gene expression in CAFs nor their proliferation rate. However, CAFs enhanced secretion of ECM-related proteins due to the tumor secretome as demonstrated by our confocal reflectance images of collagen fibers and elastic modulus results (Fig. 5), suggesting a possible post-translational mechanism of regulation of desmoplasia.

3.8. Molecular profiling of tumor-secreted factors

Based on our CM results, it is clear that tumor-secreted factors play crucial roles in CAF-induced stromal desmoplasia. To better understand the particular molecular mode of interaction present within tumor cell CM, we next performed ELISA on both types of tumor cell CM (MDA-MB-231 and MCF7) to assess the expression levels of known cytokines that participate in fibrosis, including Interleukin 4 (IL-4), Interleukin 13 (IL-13), platelet derived growth factor AA (PDGF-AA), platelet derived growth factor AB (PDGF-AB), platelet derived growth factor BB (PDGF-BB), platelet derived growth factor CC (PDGF-CC) and transforming growth factor β1 (TGF-β1) [44–46]. Based on our matrix stiffness results observed in CM experiments (Fig. 5), we hypothesized that the concentration of fibrotic factors would be significantly higher within our tumor (MDA-MB-231, MCF7) mono-culture CM as compared to their respective co-culture CM since these pro-factors are already uptaken by CAFs in the co-culture group. Additionally, we studied the secretion of the same cytokines in CM collected from CAF mono-culture to provide a broad understanding on expression of these factors by different types of cells, i.e. tumor and stromal cells. Our results showed undetectable levels of IL-4 and PDGF-CC across all the experimental conditions due to a potential low concentration of the analytes across all the samples while accurate TGF- β1 detection was obstructed due to non-specific binding of the antigen with the serum protein present in the samples (matrix effect) within our custom-based ELISA [47]. Further analysis showed expression of multiple cytokines including IL-13, PDGF-AA, and PDGF-BB in all samples (Fig. 6A). We also observed detectable levels of PDGF-AB in various conditions, although it was found to be undetectable for CAF CM (Fig. 6A). Amongst all cytokines, we notably observed a significantly higher expression of PDGF-AA and

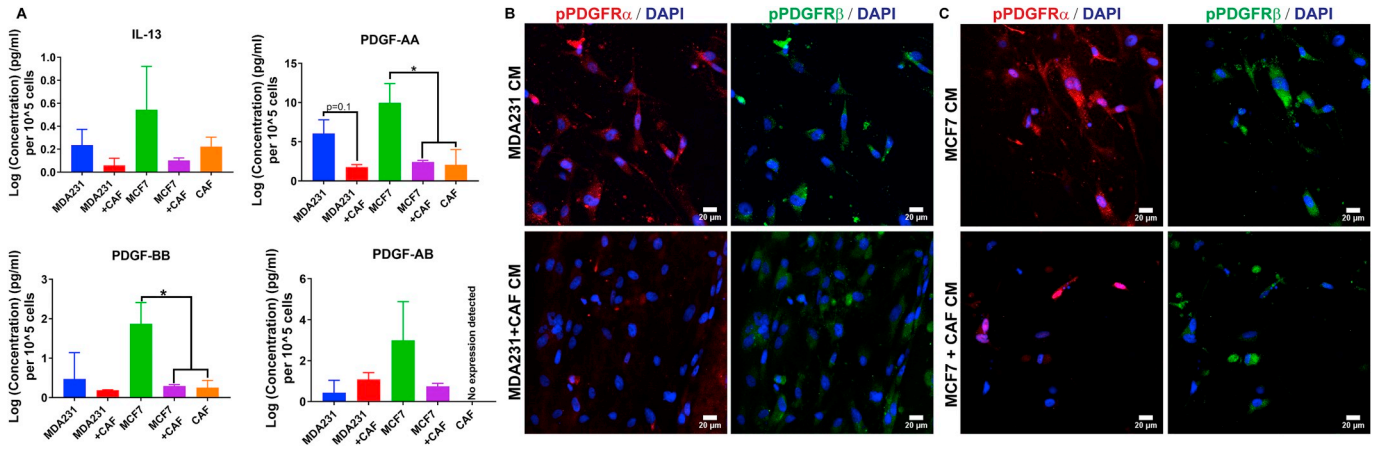

Fig. 6. Quantification of pro-fibrotic factors in tumor and stromal CM. (A) Quantification of IL-13, PDGF-AA, PDGF-BB, and PDGF-AB in CM collected from various experimental groups obtained from mono-culture of tumor cells, co-culture groups or mono-culture of CAFs. (B), (C) Representative IF showing enhanced activation of PDGFR α/β in CAFs upon incubation with CM obtained from mono-culture and co-culture of MDA-MB-231 and MCF7 cells respectively. All scale bars represent 20 μM * represents p value $<$ 0.05.

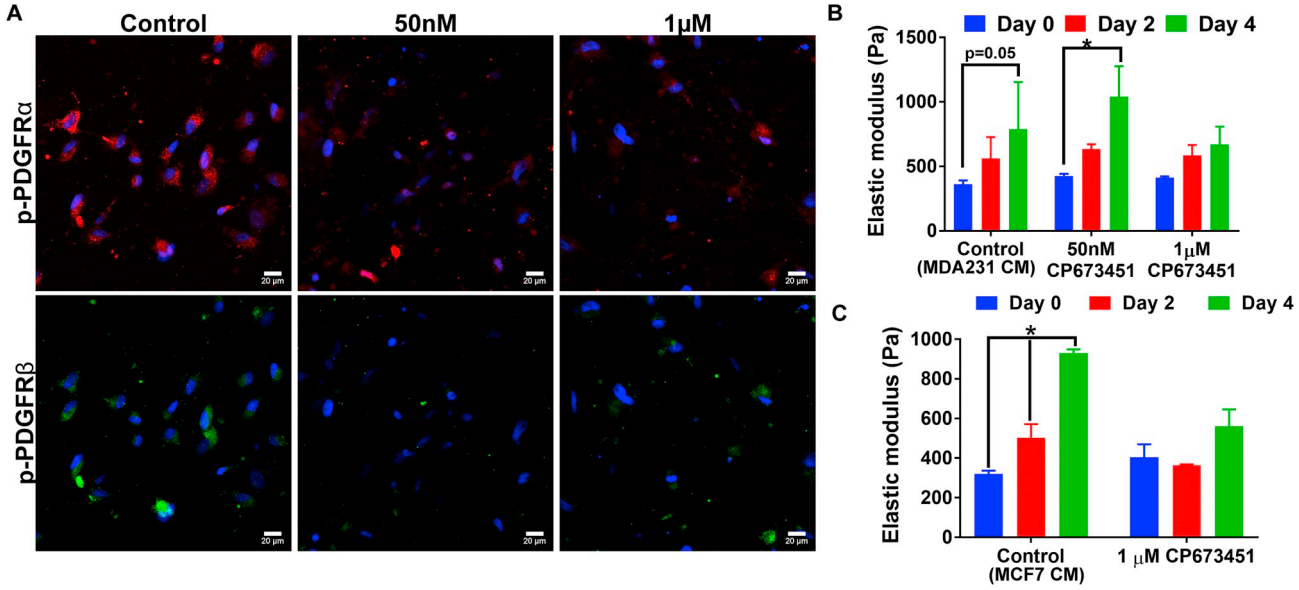

Fig. 7. The influence of PDGFR inhibitor on CAF-based desmoplasia. (A) Representative IF images showing reduced activation of PDGFR α/β receptors in CAFs upon addition of CP673451 at different concentrations in MDA-MB-231 mono-culture CM. (B), (C) Elastic modulus assessment of the matrix in CAF-only group upon incubation with (B) MDA-MB-231 and (C) MCF7 CM supplemented with different concentrations of CP673451. All scale bars represent 20 μm * represents p value $<$ 0.05.

PDGF-BB in MCF7 mono-culture CM as compared to MCF7 co-culture CM and CAF CM (Fig. 6A). We observed a similar trend for MDA-MB-231 mono-culture CM where PDGF-AA was at 3.4 times the concentration than in co-culture CM, although this result was not statistically significant (p = 0.10, p = 0.12, Fig. 6A). The demonstrated abundance of these ligands in tumor mono-culture CM as compared to co-culture CM can be speculated to be due to both prevalent expression of these ligands by tumor cells, and enhanced consumption of the ligands by the cells in the co-culture samples by a known process of ligand-receptor internalization [42,43,48]. To validate our ELISA results, we also performed IF staining for phosphorylated PDGFR α/β (Fig. 6B). Our results indicated that the activation of α and β receptors was more prominent in CAFs incubated with either MDA-MB-231 and MCF7 mono-culture CM as compared to their respective co-culture CM, further demonstrating limited availability of the PDGF ligands in co-culture CM (Fig. 6B). As shown in Supplementary Fig. 9, we observed minimal to no phosphorylation of PDGFR α/β in CAFs incubated with either DMEM-based media or CAF mono-culture CM. This indicates that PDGF ligands are potentially expressed by tumor cells which are readily available in tumor mono-culture CM but exhausted in co-culture CM.

3.9. Inhibition of PDGFR pathway in CAFs and reassessment of stromal stiffness

To validate the role of tumor-secreted PDGF-AA/-BB on CAF-induced desmoplasia, we performed a functional assessment by incubating tumor cell mono-culture CM with a concentration sweep of a specific inhibitor of PDGFRs (CP673451). We further reassessed activation of receptors and elastic modulus of the matrix in CAF-only samples across the culture period. Amongst various receptor tyrosine kinase inhibitors available, CP673451 has been observed to have 450 to 5000-fold more selectivity for PDGFRs over other receptors [49]. Appropriate concentration of CP673451 to inhibit the phosphorylation of PDGFRs depends on the cell type and has been observed to range from 1 nM to 5 μM in different cell types in numerous studies [49–51]. Based on previous studies, we utilized two different concentrations of

CP673451 (50 nM and 1 μM) to inhibit PDGFR phosphorylation in CAFs when supplemented with tumor cell mono-culture CM [50,52]. Before proceeding with measurment of elastic modulus of the stromal matrix, we also confirmed that both of these concentrations of CP673451 did not influence CAF viability as shown in Supplementary Fig. 10. Our IF results demonstrated a notable reduction in activation of the PDGF receptors in CAFs at both 50 nM and 1 μM concentrations of CP673451 in MDA-MB-231 mono-culture CM as shown in Fig. 7A. Consistent to previous results, quantitivate analysis for ECM stiffness demonstrated that the elastic modulus of the matrix significantly increased when CAFs were incubated with tumor mono-culture CM (Fig. 7B and C). At a low concentration of CP673451 (50 nM), a similar increase in elastic modulus of the matrix was observed. However, when the concentration was increased to 1 μM, no significant change in ECM stiffness was observed at day 2 and 4 of the culture as compared to day 0 (Fig. 7B). Similar observation was also made when the CAF mono-culture group was incubated with MCF7 mono-culture CM supplemented with 1 μM of CP673451 (Fig. 7C). We also compared CAF proliferation in MDA-MB-231 and MCF7 mono-culture CM in the presence of different concentrations of CP673451 (Supplementary Fig. 11) using Edu assay. Our analysis suggested that CAF proliferation was significantly reduced at 1 μM of CP673451, when compared to control MDA-MB-231 CM and 50 nM of CP673451 (Supplementary Fig. 11A and B). No significant difference was observed in CAFs proliferation between control MDA-MB-231 CM and 50nM of CP673451 (Supplementary Fig. 11A and B) Similarly for MCF7 CM, we noted a significant reduction in CAF proliferation when CP673451 was added at a concentration of 1 μM (Supplementary Fig. 11 A, C). These results suggest that inhibition of the PDGFR pathway in the presence of tumor mono-culture CM within CAFs reduces the replicative ability of CAFs, potentially reducing ECM deposition.

4. Discussion

Cancer-induced desmoplasia in various types of solid tumors leads to tumor progression, and has been associated with poor clinical outcomes [12]. CAFs are known to play a crucial role in establishing a desmoplastic tumor microenvironment by depositing various ECM proteins and increasing stromal stiffness [3]. To date, multiple studies have been performed to demonstrate the crucial role of co-culture of tumor cells and CAFs on tumor proliferation, invasion and anti-cancer drug resistance [10,29,31,53,54]. While the role of matrix biophysical properties in tumorigenicity has been well studied in various *in vivo* and *in vitro* models, there is still a technological need to quantitatively assess stromal desmoplasia during active cancer cell invasion and to further mechanistically dissect the role of tumor-stroma crosstalk on ECM dysregulation [22,24–26]. In this study, we developed a technologically advanced high-density 3D breast tumor-stroma platform, with well-defined organotypic architecture, integrated with AFM to address this knowledge gap. Due to the open-top nature of the platform, we were able to perform *in situ* analyses of the biophysical properties of stromal matrix while assessing active tumor progression. Our study was based on in-depth cellular- and molecular-level analyses to unveil key molecular regulators that participate in ECM remodeling within the context of tumor-stroma crosstalk.

Based on AFM measurements, the elastic moduli of all samples was found to be consistent in the range of 0.89–1.5 KPa on day 0 similar to the stiffness range of the healthy patient tissue (~1.13 ± 0.78 KPa) [11]. While the mono-culture groups of either tumor cells or CAFs did not show any significant changes in the matrix stiffness, the co-culture conditions of MDA-MB-231 and MCF7 cells with CAFs exhibited 2.4–3.2 times higher elastic moduli on day 4 of the culture as compared to day 0. Previous studies utilizing AFM on patient biopsies have shown that fibrotic breast cancer tissues have a bimodal distribution of stiffness such that the tumor-rich regions exhibited elastic modulus values in the range of 0.3–0.75 KPa while the stromal region exhibited a stiffer microenvironment with a very broad distribution of elastic moduli ranging from 1.5 KPa to 20 KPa [11]. Such a broad range of stiffness values obtained from patient samples can be consequential of measuring a heterogenous tissue comprising of numerous cell types (i.e. CAFs, immune cells) which could not be distinguished from the ECM during measurement. Our 3D tumor-stroma model on the other hand provided a well-controlled environment to specifically assess the elastic modulus of the stromal ECM, emerged from a specific class of stromal cells (i.e CAFs). Besides enhanced matrix stiffness within co-culture groups of tumor cells and CAFs, qRT-PCR analyses also demonstrated high expression of matrix-related genes including COL1A1, COL3A1, FN, LOX, and TGF-β as compared to the mono-culture of tumor cells. Further analysis demonstrated that CAFs were the primary source of expression of matrix-related genes as compared to either tumor cell line, thus underlining the crucial role of CAFs in ECM remodeling as also suggested in previous reports [3,28,35,36,55].

Our studies further revealed the necessary interaction between breast tumor cells and CAFs to induce a stromal desmoplastic reaction. To that end, we took a step forward by analyzing a mode of mechanism by which tumor cells and CAFs interact with each other to participate in ECM remodeling. Our CM studies suggested that tumor cells and CAFs interact with each other through paracrine signaling. We observed that tumor-secreted factors are essential to induce CAF-based desmoplasia. Similar observations have been also made in pancreatic tumors where α-SMA^{+} pancreatic stellate cells (PSCs) demonstrated enhanced proliferation upon culture with supernatants obtained from different cancer cells including MiaPaCa2, Panc1 and SW850 [56]. Additionally, synthesis of matrix proteins including collagen I and III, and fibronectin were significantly upregulated when PSCs were cultured in cancer cell supernatants, suggesting enhanced ECM remodeling [56]. Adding neutralizing antibodies against different pro-fibrotic factors including TGF-β1, FGF-2 and PDGF to cancer cells supernatants caused a significant reduction in ECM deposition [56]. Another study by Calvo et al. also demonstrated that tumor-secreted soluble factors participate in nuclear localization of the transcription factor Yes-associated protein (YAP) in normal fibroblasts (NF) transformation, proliferation and collagen deposition [57]. In this study when NFs were cultured with 4T1 cell CM, the NFs demonstrated a significant increase in gel contraction as compared to culture in DMEM-based media [57]. Additionally, CM-induced NFs significantly supported cancer cell invasion as compared to control NFs, suggesting a crucial role of tumor-secreted factors in inducing CAF-like phenotype [57]. Overall, our results demonstrate a crucial role of tumor-secreted factors that, upon binding to receptors on CAFs, get internalized and activate desmoplastic pathways to enhanced matrix deposition and stiffness.

Our ELISA analyses further highlighted significantly higher amounts of PDGF-AA and -BB ligands in tumor mono-culture CM as compared to co-culture with CAF CM. We believe that the difference in the amount of PDGF ligands between tumor mono-culture and co-culture CM can be explained by the following two rationales. Firstly, multiple studies suggested that tumor cells are the predominant source of PDGF ligands, while both tumor cells and CAFs express respective PDGFRs [48,58]. Thus, we speculate that due to the presence of both tumor cells and CAFs in the co-culture group, the rate of PDGF ligand-receptor interaction is significantly higher than that in the tumor mono-culture group. Secondly, PDGFRs have been demonstrated to get rapidly internalized when they bind to their respective ligands followed by dimerization and autophosphorylation as mentioned previously [59,60]. Wang et al. demonstrated that endosomal internalization of phosphorylated receptors is crucial in various downstream signaling pathways, including PI3K, Ras-ERK, and PLC-γ1 leading to cell survival and proliferation [59]. Thus, due to enhanced ligand-receptor interaction in co-culture conditions followed by internalization of the ligand-receptor complex, the ligands in the co-culture CM are not as readily available as compared to the mono-culture CM. While the kinetics of ligand-receptor internalization is crucial to understand the importance of the

PDGF pathway in tumor-stroma crosstalk, such an assessment is beyond the scope of the current manuscript and will be performed in our next studies.

Our study demonstrated how breast tumor cells of varied genomic make-up (i.e. MDA-MB-231 and MCF7) enhance their tumorigenicity across various hallmarks of cancer in the presence of CAFs. Delaunay triangulation analysis and live cell tracking suggested that MDA-MB-231 cells scattered more into the stroma in co-culture condition, as compared to mono-culture. These findings corroborated with one of the recent studies by Dvorak et al. who utilized MDA-MB-231 cells and co-cultured with two different populations of CAFs including WS19T and WS21T cells [61]. The authors demonstrated that when MDA-MB-231 cells were co-cultured with CM obtained from WS19T, the tumor cells depicted enhanced migratory characteristics in both 2D wound healing assays and 3D collagen matrices. On the other hand, less invasive MCF7 cells demonstrated an enhanced clustering and proliferative tendency upon co-culture with CAFs. Consistently, previous reports have also demonstrated that co-culturing MCF7 cells with CAFs enhances their proliferative ability as compared to either their mono-culture or co-culture with normal fibroblasts [62]. These studies also suggest that MCF7 cells undergo EMT in presence of CAFs thereby enhancing invasion abilities [4,62]. Such changes in migratory and proliferation patterns of MDA-MB-231 and MCF7 cells in the presence of CAFs can be attributed to both biophysical and biochemical changes induced by CAFs [36] within our platform. CAF-induced desmoplasia can be sensed by tumor cells through specific cell adhesion molecules such as integrin. Integrin binding activates an outside-in signaling cascade in the cells to bring a change in their actin cytoskeleton structure and activate various signaling pathways that have been shown to participate in cell migration, proliferation, and differentiation [35,63]. CAFs have also been implicated to assist in directional migration of tumor cells by depositing an aligned matrix due to high contractility and cell traction force. In addition to biophysical changes, CAFs also secrete certain cytokines including TGF-β, hepatocyte growth factor (HGF), and stromal cell-derived factor 1α (SDF-1α) that can regulate tumor cell migration and proliferation [35]. For instance, TGF-β overexpression by CAFs can induce tumor cells to undergo EMT which can enhance tumor migratory capabilities [64]. Other cytokines secreted by CAFs such as HGF, SDF-1α, and fibroblast growth factor (FGF) can participate in enhanced tumorigenesis by activating signaling cascades, such as MAPK, PI3K,AkT, and STAT to promote tumor stemness, proliferation and migration [64]. To differentiate the effect of biophysical cues from biochemical cues propagated by CAFs on tumor progression, a detailed mechanistic study is crucial and is a subject of our future studies.

5. Conclusion

In this work, we developed a 3D high-density organotypic tumor-stroma platform, integrated with AFM, to assess the role of crosstalk of breast cancer cells and CAFs on tumorgenicity and stromal desmoplasia. A unique feature of our work was the ability to monitor the changes in stromal stiffness and remodeling during tumor progression. We demonstrated enhanced tumor progression in the presence of CAFs and established a critical role of tumor-stroma crosstalk on ECM desmoplasia. Our studies specifically demonstrated that the tumor secretome is the primary source of pro-fibrotic cytokines such that the elastic modulus of stromal matrix was significantly elevated when incubated with tumor conditioned media (CM). We detected higher levels of PDGF-AA and -BB ligands in CM from MDA-MB-231 and MCF7 cells as compared to CM from their respective co-culture with CAFs. We further showed a critical role of PDGF signaling in CAF-based desmoplasia, where inhibition of the activity of PDGFRs in CAFs, led to attenuation of stromal matrix stiffness. Overall, this study provides a unique system based on a 3D microengineered organotypic tumor microenvironment model, integrated with AFM, which could be broadly utilized for numerous mechanistic studies, within the context of tumor-stromal crosstalk, as well as anti-cancer drug discovery.

Data availability

The associated code and data utilized in our study is available to the readers of the journal.

CRediT authorship contribution statement

Harpinder Saini: Conceptualization, Methodology, Validation, Formal analysis, Investigation, Data curation, Writing - original draft, Writing - review & editing, Visualization. **Kiarash Rahmani Eliato:** Methodology, Validation, Formal analysis, Investigation, Writing - original draft. **Jaimeson Veldhuizen:** Methodology, Investigation, Formal analysis, Writing - review & editing. **Azadeh Zare:** Investigation, Formal analysis. **Mayar Allam:** Investigation. **Casey Silva:** Investigation. **Alex Kratz:** Investigation. **Danh Truong:** Methodology. **Ghassan Mouneimne:** Conceptualization. **Joshua LaBaer:** Conceptualization, Writing - review & editing. **Robert Ros:** Conceptualization, Resources, Writing - review & editing, Project administration, Funding acquisition. **Mehdi Nikkhah:** Conceptualization, Methodology, Resources, Writing - review & editing, Supervision, Project administration, Funding acquisition.

Declaration of competing interest

The authors declare that they have no known competing financial interests or personal relationships that could have appeared to influence the work reported in this paper.

Acknowledgements

The authors would like to acknowledge National Science Foundation (NSF) CBET Awards #1510700 and #1914680 (MN), National Cancer Institute (NCI) grant R01 CA196885-01 (GM) and ASU Fulton Undergraduate Research Initiative(FURI) for supporting this study. The authors declare no competing interests.

Appendix A. Supplementary data

Supplementary data to this article can be found online at https://doi.org/10.1016/j.biomaterials.2020.119975.

References

[1] R.L. Siegel, K.D. Miller, A. Jemal, Cancer statistics, 2019, CA, Canc. J. Clin. 69 (1) (2019) 7–34.
[2] F.R. Balkwill, M. Capasso, T. Hagemann, The tumor microenvironment at a glance, J. Cell Sci. 125 (Pt 23) (2012) 5591–5596.
[3] R. Kalluri, The biology and function of fibroblasts in cancer, Nat. Rev. Canc. 16 (9) (2016) 582–598.
[4] Y. Yu, C.H. Xiao, L.D. Tan, Q.S. Wang, X.Q. Li, Y.M. Feng, Cancer-associated fibroblasts induce epithelial-mesenchymal transition of breast cancer cells through paracrine TGF-beta signalling, Br. J. Canc. 110 (3) (2014) 724–732.
[5] S. Wen, Y. Hou, L. Fu, L. Xi, D. Yang, M. Zhao, Y. Qin, K. Sun, Y. Teng, M. Liu, Cancer-associated fibroblast (CAF)-derived IL32 promotes breast cancer cell invasion and metastasis via integrin β3–p38 MAPK signalling, Canc. Lett. 442 (2019) 320–332.
[6] L. Monteran, N. Erez, The dark side of fibroblasts: cancer-associated fibroblasts as mediators of immunosuppression in the tumor microenvironment, Front. Immunol. 10 (2019) 1835.
[7] N. Cohen, O. Shani, Y. Raz, Y. Sharon, D. Hoffman, L. Abramovitz, N. Erez, Fibroblasts drive an immunosuppressive and growth-promoting microenvironment in breast cancer via secretion of Chitinase 3-like 1, Oncogene 36 (31) (2017) 4457–4468.
[8] A. Orimo, P.B. Gupta, D.C. Sgroi, F. Arenzana-Seisdedos, T. Delaunay, R. Naeem, V.J. Carey, A.L. Richardson, R.A. Weinberg, Stromal fibroblasts present in invasive human breast carcinomas promote tumor growth and angiogenesis through elevated SDF-1/CXCL12 secretion, Cell 121 (3) (2005) 335–348.
[9] K. Takai, A. Le, V.M. Weaver, Z. Werb, Targeting the cancer-associated fibroblasts

as a treatment in triple-negative breast cancer, Oncotarget 7 (50) (2016) 82889–82901.
[10] N. Peela, D. Truong, H. Saini, H. Chu, S. Mashaghi, S.L. Ham, S. Singh, H. Tavana, B. Mosadegh, M. Nikkhah, Advanced biomaterials and microengineering technologies to recapitulate the stepwise process of cancer metastasis, Biomaterials 133 (2017) 176–207.
[11] M. Plodinec, M. Loparic, C.A. Monnier, E.C. Obermann, R. Zanetti-Dallenbach, P. Oertle, J.T. Hyotyla, U. Aebi, M. Bentires-Alj, R.Y. Lim, C.A. Schoenenberger, The nanomechanical signature of breast cancer, Nat. Nanotechnol. 7 (11) (2012) 757–765.
[12] I. Acerbi, L. Cassereau, I. Dean, Q. Shi, A. Au, C. Park, Y.Y. Chen, J. Liphardt, E.S. Hwang, V.M. Weaver, Human breast cancer invasion and aggression correlates with ECM stiffening and immune cell infiltration, Integr Biol (Camb) 7 (10) (2015) 1120–1134.
[13] D. Truong, J. Puleo, A. Llave, G. Mouneimne, R.D. Kamm, M. Nikkhah, Breast cancer cell invasion into a three dimensional tumor-stroma microenvironment, Sci. Rep. 6 (2016) 34094.
[14] C.M. Kraning-Rush, S.P. Carey, M.C. Lampi, C.A. Reinhart-King, Microfabricated collagen tracks facilitate single cell metastatic invasion in 3D, Integr Biol (Camb) 5 (3) (2013) 606–616.
[15] D. Truong, R. Fiorelli, E.S. Barrientos, E.L. Melendez, N. Sanai, S. Mehta, M. Nikkhah, A three-dimensional (3D) organotypic microfluidic model for glioma stem cells – vascular interactions, Biomaterials 198 (2019) 63–77.
[16] S. Nagaraju, D. Truong, G. Mouneimne, M. Nikkhah, Microfluidic tumor–vascular model to study breast cancer cell invasion and intravasation, Advanced Healthcare Materials 7 (9) (2018) 1701257.
[17] N. Peela, E.S. Barrientos, D. Truong, G. Mouneimne, M. Nikkhah, Effect of suberoylanilide hydroxamic acid (SAHA) on breast cancer cells within a tumor–stroma microfluidic model, Integrative Biol. 9 (12) (2017) 988–999.
[18] S. Chung, R. Sudo, P.J. Mack, C.-R. Wan, V. Vickerman, R.D. Kamm, Cell migration into scaffolds under co-culture conditions in a microfluidic platform, Lab Chip 9 (2) (2009) 269–275.
[19] I.K. Zervantonakis, S.K. Hughes-Alford, J.L. Charest, J.S. Condeelis, F.B. Gertler, R.D. Kamm, Three-dimensional microfluidic model for tumor cell intravasation and endothelial barrier function, Proc. Natl. Acad. Sci. Unit. States Am. 109 (34) (2012) 13515–13520.
[20] S.M. Ehsan, K.M. Welch-Reardon, M.L. Waterman, C.C.W. Hughes, S.C. George, A three-dimensional in vitro model of tumor cell intravasation, Integrative Biol. 6 (6) (2014) 603–610.
[21] V.S. Shirure, Y. Bi, M.B. Curtis, A. Lezia, M.M. Goedegebuure, S.P. Goedegebuure, R. Aft, R.C. Fields, S.C. George, Tumor-on-a-chip platform to investigate progression and drug sensitivity in cell lines and patient-derived organoids, Lab Chip 18 (23) (2018) 3687–3702.
[22] N. Peela, F.S. Sam, W. Christenson, D. Truong, A.W. Watson, G. Mouneimne, R. Ros, M. Nikkhah, A three dimensional micropatterned tumor model for breast cancer cell migration studies, Biomaterials 81 (2016) 72–83.
[23] M.H. Zaman, L.M. Trapani, A.L. Sieminski, D. MacKellar, H. Gong, R.D. Kamm, A. Wells, D.A. Lauffenburger, P. Matsudaira, Migration of tumor cells in 3D matrices is governed by matrix stiffness along with cell-matrix adhesion and proteolysis, Proc. Natl. Acad. Sci. Unit. States Am. 103 (29) (2006) 10889–10894.
[24] M. Ehrbar, A. Sala, P. Lienemann, A. Ranga, K. Mosiewicz, A. Bittermann, S.C. Rizzi, F.E. Weber, M.P. Lutolf, Elucidating the role of matrix stiffness in 3D cell migration and remodeling, Biophys. J. 100 (2) (2011) 284–293.
[25] O. Chaudhuri, S.T. Koshy, C. Branco da Cunha, J.W. Shin, C.S. Verbeke, K.H. Allison, D.J. Mooney, Extracellular matrix stiffness and composition jointly regulate the induction of malignant phenotypes in mammary epithelium, Nat. Mater. 13 (10) (2014) 970–978.
[26] N.R. Lang, K. Skodzek, S. Hurst, A. Mainka, J. Steinwachs, J. Schneider, K.E. Aifantis, B. Fabry, Biphasic response of cell invasion to matrix stiffness in 3-dimensional biopolymer networks, Acta Biomater. 13 (2015) 61–67.
[27] L.C. Bahlmann, L.J. Smith, M.S. Shoichet, Designer biomaterials to model cancer cell invasion in vitro: predictive tools or just pretty pictures?, Adv. Funct. Mater. n/a(n/a) 1909032.
[28] A. Santi, F.G. Kugeratski, S. Zanivan, Cancer associated fibroblasts: the architects of stroma remodeling, Proteomics 18 (5–6) (2018) e1700167.
[29] D.D. Truong, A. Kratz, J.G. Park, E.S. Barrientos, H. Saini, T. Nguyen, B. Pockaj, G. Mouneimne, J. LaBaer, M. Nikkhah, A human organotypic microfluidic tumor model permits investigation of the interplay between patient-derived fibroblasts and breast cancer cells, Canc. Res. 79 (12) (2019) 3139–3151.
[30] C.M. Nelson, J.L. Inman, M.J. Bissell, Three-dimensional lithographically defined organotypic tissue arrays for quantitative analysis of morphogenesis and neoplastic progression, Nat. Protoc. 3 (4) (2008) 674–678.
[31] H. Saini, K. Rahmani Eliato, C. Silva, M. Allam, G. Mouneimne, R. Ros, M. Nikkhah, The role of desmoplasia and stromal fibroblasts on anti-cancer drug resistance in a microengineered tumor model, Cell. Mol. Bioeng. 11 (5) (2018) 419–433.
[32] J.L. Hutter, J. Bechhoefer, Calibration of atomic-force microscope tips, Rev. Sci. Instrum. 64 (7) (1993) 1868–1873.
[33] R.E. Mahaffy, C.K. Shih, F.C. MacKintosh, J. Käs, Scanning probe-based frequency-dependent microrheology of polymer gels and biological cells, Phys. Rev. Lett. 85 (4) (2000) 880–883.
[34] T. Liu, C. Han, S. Wang, P. Fang, Z. Ma, L. Xu, R. Yin, Cancer-associated fibroblasts: an emerging target of anti-cancer immunotherapy, J. Hematol. Oncol. 12 (1) (2019) 86.
[35] T. Liu, L. Zhou, D. Li, T. Andl, Y. Zhang, Cancer-associated fibroblasts build and secure the tumor microenvironment, Frontiers Cell Dev. Biol. 7 (60) (2019).
[36] P. Cirri, P. Chiarugi, Cancer associated fibroblasts: the dark side of the coin, Am. J. Canc. Res. 1 (4) (2011) 482–497.
[37] R. Kalluri, M. Zeisberg, Fibroblasts in cancer, Nat. Rev. Canc. 6 (5) (2006) 392–401.
[38] B. Nawrocki Raby, M. Polette, C. Gilles, C. Clavel, K. Strumane, M. Matos, J.-M. Zahm, F. Van Roy, N. Bonnet, P. Birembaut, Quantitative cell dispersion analysis: new test to measure tumor cell aggressiveness, Int. J. Canc. 93 (5) (2001) 644–652.
[39] P.A. Kenny, G.Y. Lee, C.A. Myers, R.M. Neve, J.R. Semeiks, P.T. Spellman, K. Lorenz, E.H. Lee, M.H. Barcellos-Hoff, O.W. Petersen, J.W. Gray, M.J. Bissell, The morphologies of breast cancer cell lines in three-dimensional assays correlate with their profiles of gene expression, Molecular Oncology 1 (1) (2007) 84–96.
[40] H. Hatzikirou, D. Basanta, M. Simon, K. Schaller, A. Deutsch, 'Go or Grow': the key to the emergence of invasion in tumour progression? Math. Med. Biol.: A Journal of the IMA 29 (1) (2012) 49–65.
[41] S. Nakagawa, Y. Miki, M. Miyashita, S. Hata, Y. Takahashi, Y. Rai, Y. Sagara, Y. Ohi, H. Hirakawa, K. Tamaki, T. Ishida, M. Watanabe, T. Suzuki, N. Ohuchi, H. Sasano, Tumor microenvironment in invasive lobular carcinoma: possible therapeutic targets, Breast Canc. Res. Treat. 155 (1) (2016) 65–75.
[42] J. Pahara, H. Shi, X. Chen, Z. Wang, Dimerization drives PDGF receptor endocytosis through a C-terminal hydrophobic motif shared by EGF receptor, Exp. Cell Res. 316 (14) (2010) 2237–2250.
[43] K. Jastrzębski, D. Zdżalik-Bielecka, A. Mamińska, Y. Kalaidzidis, C. Hellberg, M. Miaczynska, Multiple routes of endocytic internalization of PDGFRβ contribute to PDGF-induced STAT3 signaling, J. Cell Sci. 130 (3) (2017) 577–589.
[44] C. Jakubzick, S.L. Kunkel, R.K. Puri, C.M. Hogaboam, Therapeutic targeting of IL-4- and IL-13-responsive cells in pulmonary fibrosis, Immunol. Res. 30 (3) (2004) 339–349.
[45] J.C. Bonner, Regulation of PDGF and its receptors in fibrotic diseases, Cytokine Growth Factor Rev. 15 (4) (2004) 255–273.
[46] T. Wynn, Cellular and molecular mechanisms of fibrosis, J. Pathol. 214 (2) (2008) 199–210.
[47] R.M. Crisino, L. Luo, B. Geist, J. Zoghbi, F. Spriggs, Matrix effect in ligand-binding assay: the importance of evaluating emerging technologies, Bioanalysis 6 (8) (2014) 1033–1036.
[48] M. Bartoschek, K. Pietras, PDGF family function and prognostic value in tumor biology, Biochem. Biophys. Res. Commun. 503 (2) (2018) 984–990.
[49] W.G. Roberts, P.M. Whalen, E. Soderstrom, G. Moraski, J.P. Lyssikatos, H.-F. Wang, B. Cooper, D.A. Baker, D. Savage, D. Dalvie, J.A. Atherton, S. Ralston, R. Szewc, J.C. Kath, J. Lin, C. Soderstrom, G. Tkalcevic, B.D. Cohen, V. Pollack, W. Barth, W. Hungerford, E. Ung, Antiangiogenic and antitumor activity of a selective PDGFR tyrosine kinase inhibitor CPA673451, Cancer Research 65 (3) (2005) 957–966.
[50] K. Aoto, K. Ito, S. Aoki, Complex formation between platelet-derived growth factor receptor β and transforming growth factor β receptor regulates the differentiation of mesenchymal stem cells into cancer-associated fibroblasts, Oncotarget 9 (75) (2018).
[51] Y. Xi, M. Chen, X. Liu, Z. Lu, Y. Ding, D. Li, CP-673451, a platelet-derived growth-factor receptor inhibitor, suppresses lung cancer cell proliferation and migration, OncoTargets Ther. 7 (2014) 1215–1221.
[52] S. Álvarez-Teijeiro, C. García-Inclán, M.Á. Villaronga, P. Casado, F. Hermida-Prado, R. Granda-Díaz, J.P. Rodrigo, F. Calvo, N. Del-Río-Ibisate, A. Gandarillas, F. Morís, M. Hermsen, P. Cutillas, J.M. García-Pedrero, Factors secreted by cancer-associated fibroblasts that sustain cancer stem properties in head and neck squamous carcinoma cells as potential therapeutic targets, Cancers 10 (9) (2018) 334.
[53] E.L.S. Fong, D.A. Harrington, M.C. Farach-Carson, H. Yu, Heralding a new paradigm in 3D tumor modeling, Biomaterials 108 (2016) 197–213.
[54] M. Plaster, S. Singh, H. Tavana, Fibroblasts promote proliferation and matrix invasion of breast cancer cells in Co-culture models, Advanced Therapeutics 2 (11) (2019) 1900121.
[55] S. Singh, L.A. Ray, P. Shahi Thakuri, S. Tran, M.C. Konopka, G.D. Luker, H. Tavana, Organotypic breast tumor model elucidates dynamic remodeling of tumor microenvironment, Biomaterials 238 (2020) 119853.
[56] M.G. Bachem, M. Schünemann, M. Ramadani, M. Siech, H. Beger, A. Buck, S. Zhou, A. Schmid-Kotsas, G. Adler, Pancreatic carcinoma cells induce fibrosis by stimulating proliferation and matrix synthesis of stellate cells, Gastroenterology 128 (4) (2005) 907–921.
[57] F. Calvo, N. Ege, A. Grande-Garcia, S. Hooper, R.P. Jenkins, S.I. Chaudhry, K. Harrington, P. Williamson, E. Moeendarbary, G. Charras, E. Sahai, Mechanotransduction and YAP-dependent matrix remodelling is required for the generation and maintenance of cancer-associated fibroblasts, Nat. Cell Biol. 15 (6) (2013) 637–646.
[58] C.-H. Heldin, J. Lennartsson, B. Westermark, Involvement of platelet-derived growth factor ligands and receptors in tumorigenesis, J. Intern. Med. 283 (1) (2018) 16–44.
[59] Y. Wang, S.D. Pennock, X. Chen, A. Kazlauskas, Z. Wang, Platelet-derived growth factor receptor-mediated signal transduction from endosomes, J. Biol. Chem. 279 (9) (2004) 8038–8046.
[60] C.-H. Heldin, Targeting the PDGF signaling pathway in tumor treatment, Cell Commun. Signal. 11 (1) (2013) 97.
[61] K.M. Dvorak, K.M. Pettee, K. Rubinic-Minotti, R. Su, A. Nestor-Kalinoski, K.M. Eisenmann, Carcinoma associated fibroblasts (CAFs) promote breast cancer motility by suppressing mammalian diaphanous-related formin-2 (mDia2), PloS One 13 (3) (2018) e0195278.
[62] P.S. Soon, E. Kim, C.K. Pon, A.J. Gill, K. Moore, A.J. Spillane, D.E. Benn, R.C. Baxter, Breast cancer-associated fibroblasts induce epithelial-to-mesenchymal transition in breast cancer cells, Endocr. Relat. Canc. 20 (1) (2013) 1–12.
[63] P. Friedl, K. Wolf, Plasticity of cell migration: a multiscale tuning model, JCB (J. Cell Biol.) 188 (1) (2009) 11–19.

[64] G.S. Karagiannis, T. Poutahidis, S.E. Erdman, R. Kirsch, R.H. Riddell, E.P. Diamandis, Cancer-associated fibroblasts drive the progression of metastasis through both paracrine and mechanical pressure on cancer tissue, Mol. Canc. Res. 10 (11) (2012) 1403–1418.

[65] J Staunton, B Doss, S Lindsay, R Ros, Correlating confocal microscopy and atomic force indentation reveals metastatic cancer cells stiffen during invasion into collagen I matrices, Scientific Reports 6 (19686) (2016).

[66] Masako Yamashita, Tomoko Ogawa, Xinhui Zang, Noriko Hanamura, Yuma Kashikura, Mitsuyuki Takamura, Misao Yoneda, Taizo Shiraishi, Role of stromal myofibroblasts in invasive breast cancer: stromal expression of alpha-smooth muscle actin correlates with worse clinical outcome, Breast Cancer 19 (2012) 170–176.